

CONFIDENTIAL

72105

NASA TM X-281

Classification changed to declassified
effective 1 April 1982 under
authority of NASA COM 52 by
[Signature]



N63-13899
code 1

TECHNICAL MEMORANDUM

X-281

FLIGHT TESTS OF A TWIN-DUCT INDUCTION SYSTEM FOR
A MACH NUMBER RANGE OF 0.78 TO 2.07

By Jack Nugent and Bruce G. Powers

Flight Research Center
Edwards, Calif.



CLASSIFIED BY [redacted] - [redacted]

This material contains information affecting the national defense of the United States within the meaning of the espionage laws, Title 18, U.S.C., Secs. 793 and 794, the transmission or revelation of which in any manner to an unauthorized person is prohibited by law.

NATIONAL AERONAUTICS AND SPACE ADMINISTRATION

WASHINGTON

September 1960

CONFIDENTIAL

NASA TM X-281

449

UNCLASSIFIED
CONFIDENTIAL

NATIONAL AERONAUTICS AND SPACE ADMINISTRATION

TECHNICAL MEMORANDUM X-281

FLIGHT TESTS OF A TWIN-DUCT INDUCTION SYSTEM FOR

A MACH NUMBER RANGE OF 0.78 TO 2.07*

By Jack Nugent and Bruce G. Powers

SUMMARY

Flight tests of a twin-duct induction system over a Mach number range from about 0.78 to about 2.07 during quasi-steady operation indicated that in the Mach number range from about 1.05 to about 1.55 the 40,000-foot data exhibited about a $1\frac{1}{2}$ -percent higher total-pressure recovery than did the 26,000-foot data. This result was obtained for very similar subcritical shock-wave configuration and identical bypass configuration at trim angle of attack. The 26,000-foot data showed significantly lower distortion, however. A total-pressure recovery of about 95 percent and a distortion parameter of about 15 percent were noted for the 40,000-foot data at a Mach number of 1.55. The 40,000-foot data and 55,000-foot data showed essentially the same recovery for very similar shock-wave configuration and an increased bypass configuration at trim angle of attack. A value of about 81 percent was noted for a Mach number of 2.05 for both sets of data. A distortion of 33 percent was obtained for the 55,000-foot data at a Mach number of about 1.24 during supercritical operation.

At a Mach number of 1.7, area-weighted pressure recovery decreased from about 91 percent to about 88 percent as angle of attack increased from 3° to 7°, whereas the distortion parameter decreased from 19 percent to 15 percent as angle of attack increased above 2°. Angle of attack produced only slight effects at lower Mach numbers. Local total-pressure recovery exhibited symmetry about the vertical center line of the engine face for all data. Highest total-pressure recovery was obtained at the 3 o'clock and 9 o'clock rake positions, with lowest recovery obtained at the bottom of the duct during level flight. For the same Mach number all test data showed essentially the same cone-pressure profiles. Shock-boundary-layer interaction along the cone surface occurred for the 40,000-foot data and the 55,000-foot data for Mach numbers of 1.5 and greater. This result affected the cone-surface pressure distribution. During ground-run operation, a recovery of about 88 percent and a distortion parameter of 10 percent were obtained for maximum engine demand.

*Title, Unclassified.

CONFIDENTIAL

INTRODUCTION

As the speeds of jet aircraft increase in the supersonic region between a Mach number of about 1.5 and 2.0, the simple normal-shock inlet is replaced by inlets using supersonic compression. Both two-dimensional and three-dimensional systems are in use, with provision for variable geometry in some cases. In addition, variable-area duct bypass systems may be employed for engine-inlet matching over this Mach number range. The use of variable geometry in an induction system requires auxiliary mechanism which adds weight, consumes space, and increases the complexity of the airplane. These penalties must be weighed against the increased aerodynamic efficiency afforded by the variable geometry. Consequently, there are different degrees of variable geometry in the induction systems of present-day airplanes corresponding to the several solutions of the induction-system-design problem. Basically, any induction system should yield high performance and operate compatibly with the engine over the flight environment. It is of interest, therefore, to examine the induction system of a current airplane as an aid for future designs.

Tests were made at the NASA Flight Research Center at Edwards, Calif., on a supersonic fighter airplane with twin half-conical fuselage side inlets. The inlets are of fixed geometry designed for a Mach number of 2.0; however, a three-position bypass system is employed. This system is simple compared to other solutions of the induction-system-design problem. During the initial flight-testing program, twin-duct instability and consequent nonsteady flow were encountered at a Mach number near 1.9 (ref. 1). The present tests were made under conditions of quasi-steady flow. Both test series were performed with a larger bypass area than is recommended by the manufacturer for the production version of this airplane. Data were obtained over a Mach number range from 0.78 to 2.07 and at altitudes ranging from 26,000 to 55,000 feet. Ground-run data were also obtained.

SYMBOLS

A	area, sq ft
A _c	capture area, both inlets, 763 sq in.
A _{de}	diffuser-exit area, 830 sq in.
A _{th}	throat area, both inlets, 543 sq in.
D	distortion parameter, $\frac{(H_{l_{\max}} - H_{l_{\min}})}{H_{de}}$

- H_{de} area-weighted diffuser-exit total pressure, lb/sq ft
- H_{de}/H_0 area-weighted total-pressure recovery
- H_l local total pressure, lb/sq ft
- H_0 free-stream total pressure, lb/sq ft
- H_l/H_0 local total-pressure-recovery factor
- M free-stream Mach number
- M_i Mach number in inlet plane
- M_l Mach number in front of inlet cone

m/m_0 mass-flow ratio, $\frac{\left(\frac{W_{de}\sqrt{\theta}}{\delta}\right)\left(\frac{H_{de}}{H_0}\right)}{A_c \left[\frac{85.5M}{\frac{\gamma+1}{\left(1 + \frac{\gamma-1}{2} M^2\right)^{2(\gamma-1)}}} \right]}$ (ref. 2)

m/m^* ratio of actual air flow to choking air flow at inlet throat,

$$\frac{W_{de}}{(0.532)H_0 A_{th} \sqrt{T}}$$

$N/\sqrt{\theta}$ engine corrected speed, rpm

$O_1 \dots O_5$ static-pressure orifices along cone

P_0 free-stream static pressure, lb/sq ft

P/P_0 static-pressure ratio

R Reynolds number, based on free-stream conditions and diameter of a circle equal to capture area

S_1, S_2	fuselage static-pressure orifices ahead of inlet
T	total temperature (assumed equal to free-stream total temperature), $^{\circ}R$
t	time, sec
W_{de}	diffuser-exit air flow, lb/sec
$\frac{W_{de}\sqrt{\theta}}{\delta}$	diffuser-exit corrected air flow, lb/sec
α	airplane angle of attack, deg
γ	ratio of specific heats
θ_S	effective conical-compression semiangle, deg

Subscripts:

max	maximum
min	minimum

Unless otherwise specified, the term "Mach number" refers to free-stream Mach number.

AIRPLANE AND PROPULSION SYSTEM

The test airplane is a fighter type with a maximum speed capability of a Mach number of about 2.0. Figure 1 is a photograph of the airplane, and figure 2 is a three-view drawing. Physical details are given in table I.

A schematic drawing of the internal-flow system is shown in figure 3. Supersonic compression is achieved in each inlet by a conical shock generated by a 25° semiangle half cone. The conical shock falls slightly ahead of the cowl lip at a Mach number of 2.0. The half cone is undercut from the apex to the inboard cowl section of the inlet for fuselage boundary-layer control (fig. 4(a)). Figure 4(b) shows the duct-area distribution. Photographs of the diffuser entry and exit are presented in figures 5(a) and 5(b), respectively. Cone-surface boundary layer is controlled at each inlet throat by means of a flush slot (fig. 5(a)) and is discharged through a sonic exit beneath the

fuselage. The two ducts remain separated approximately to the engine face, as shown in figure 5(b). Also shown in figure 5(b) are the variable-position bypass doors which regulate the air flow for operation of the ejector nozzle and inlet mass-flow control; all of the bypass air was used in the ejector nozzle.

The engine is of the axial-flow type with a 17-stage compressor. The first six rows of the stator vanes and the inlet-guide vanes are varied as a function of corrected engine speed for surge suppression at part-speed operation. The full-open position is attained over about 92-percent power setting. For these tests the inlet guide vanes remained essentially at the full-open position. The exhaust nozzle is a variable-ejector type infinitely variable between minimum and maximum settings. The engine speed is held constant at the rated value of 7,460 rpm for the military setting and for the several afterburner throttle settings. The engine used for the present investigation, as well as production engines, has an automatic device to maintain minimum speed at or above 7,460 rpm for any throttle position. The device functions only for Mach numbers above about 1.86 and aids in surge suppression.

To relieve the main inlets of some of the engine and ejector air requirements during take-off and low-speed operation, automatic aspirator or "suck in" doors are utilized. The doors, located in the fuselage near the engine compartment, are arranged to open inward to admit outside air whenever engine-compartment pressure is less than ambient pressure (fig. 6).

INSTRUMENTATION

Measurements of induction-system pressures were obtained at the engine compressor face, the left-inlet cone, and the left side of the fuselage immediately upstream of the cone. Figure 7 is a photograph of the rake installation used to measure the total and static pressure of the air entering the engine. The rakes were installed radially at 60° intervals, and the total-pressure tubes were placed in the center of equal-area annular sectors. Static pressures were measured on the surface of the center accessory housing at the locations of the 3 o'clock and 9 o'clock rakes. Total and static pressures were measured also for the bypass air. The pressures on the left inlet cone, static-pressure orifices O_1 to O_5 , and on the fuselage, static-pressure orifices S_1 and S_2 , are detailed in figure 8. Most of the pressures were recorded on standard NASA 12-cell pressure recorders. Several of the engine-face total pressures were sensed by temperature-compensated pressure transducers and were recorded on an oscillograph. Engine speed was also measured.

A standard NASA airspeed tube measured free-stream total and static pressure from a boom mounted on the airplane nose. Angle of attack and sideslip were also measured by vanes mounted on the boom. Free-stream

total temperature was measured by a shielded resistance-type probe mounted on the fuselage. Mach number was calibrated by the photodolite method.

All instruments were synchronized by a common timer.

ACCURACY

Mach number is accurate to within ± 0.02 transonically and ± 0.01 for the higher supersonic speeds. Angle of attack was corrected for inertial boom bending and airplane pitching velocity and is accurate to within $\pm 0.5^\circ$. The values of area-weighted total-pressure recovery H_{de}/H_0 show repeatability to within 1 percent and the values of distortion parameter D show repeatability to within $1\frac{1}{2}$ percent for comparable flight conditions.

The corrected airflow $\frac{W_{de}\sqrt{\theta}}{\delta}$ was obtained from the engine manufacturer's air-flow curves (ref. 3) which were suitably modified for the airplane bypass areas used. This parameter was checked on the ground and was found to be accurate to within 1 percent for the higher corrected engine speeds. Diffuser-exit area-weighted total-pressure recovery H_{de}/H_0 was obtained by using an arithmetic average of the area-spaced compressor-face probes and bypass-area total-pressure readings. The parameter is essentially an area-weighted value despite the inclusion of the latter readings.

DATA ANALYSIS

The data of reference 4 show that the local flow entering the inlet differs from the free stream in both Mach number and direction. In addition, the flow is nonuniform across the inlet. For analysis purposes a local Mach number M_1 was calculated by using free-stream total pressure and the static pressure indicated by orifice S_2 (fig. 8). Preliminary flight analysis and schlieren photographs (ref. 5) indicate sufficient boundary-layer flow over the apex of the cone to affect the conical-compression angle for an attached conical shock. Again, for analysis purposes, an effective conical angle was determined from plots similar to those of figure 9. By using the local Mach number and the charts of reference 6, conical-compression ratios were calculated for several cone angles near 25° and plotted against time for a given run.

The pressure ratio O_1/P_0 was also plotted in figure 9. The effective cone for a given time was assumed to occur at the intersection of the observed and calculated curves. The effective cone angle varied with flight conditions and was generally less than 25° .

After determining the local Mach number, it was possible to calculate pressure recovery for a given shock system. The nature of the shock system was inferred from the cone pressures. For a normal-shock system, normal-shock charts were used (ref. 6). For an attached conical shock during subcritical flow a two-shock recovery was calculated by using the approximate method given in reference 7. Inlet Mach number M_i was determined from the calculated total-pressure recovery through the shock system and the reading of orifice O_4 . For subsonic Mach numbers, free-stream total pressure H_0 was used to calculate M_i .

TESTS

Acceleration maneuvers were made with the test airplane from subsonic Mach numbers to terminal Mach numbers at altitudes of about 26,000 feet and about 40,000 feet in maximum afterburning power. A deceleration from a Mach number of 2.07 to a Mach number of about 1.2 was made at an altitude of about 55,000 feet. In addition, push-down-turn maneuvers were obtained through the Mach number range at an altitude of about 40,000 feet. Below a Mach number of about 1.5 the bypass area was normally kept at a nominal value of 44 square inches. Above a Mach number of about 1.5 the bypass area was increased manually by the pilot to a nominal value of 91 square inches for the speed run made at an altitude of 40,000 feet. This bypass area was also used for the entire deceleration run. In the production version of this airplane the bypass area is kept at 44 square inches for all flight speeds. Supercritical inlet flow is never obtained. At a bypass area of 91 square inches in the present tests, supercritical inlet flow was obtained in some intervals. The data were obtained under quasi-steady conditions with no evidence of the large asymmetric twin-duct flows obtained in the investigation of reference 1. The Mach number of the tests ranged from 0.78 to 2.07, and the altitude ranged from 26,000 to 55,000 feet. The test range of Reynolds number R extended from 3.1×10^6 to about 15.6×10^6 . Sideslip angle was negligible for these tests. Static data were obtained from a ground run.

TEST RESULTS

Figures 10 and 11 present time histories of the accelerations at altitudes of 26,000 feet and 40,000 feet, respectively. Presented are

the several induction-system, engine, and airplane parameters. As indicated in figure 10(a) the throttle was actuated at $t = 10$ seconds and held at the maximum setting until $t = 235$ seconds. Free-stream and local Mach number increased from $t = 0$ to $t = 235$ seconds when the throttle was reduced. Upon throttle advance, inlet Mach number shows an increase above $M = 0.8$, with sonic speed reached at $t = 43$ seconds. A steady decrease is indicated beyond $t = 55$ seconds until $t = 235$ seconds when the throttle was reduced. Distortion D (fig. 10(b)) remains essentially steady for a fixed throttle position, whereas area-weighted pressure recovery approaches the calculated values with decrease in inlet Mach number. Cone pressures O_3/P_0 , O_4/P_0 , and O_5/P_0 show steady increase with increase in Mach number. The large pressure increment noted between O_2/P_0 and O_3/P_0 near the latter part of the run indicates the terminal normal shock to be between orifice O_2 and O_3 .

The data of figures 11(a) and (b) show essentially the same trends as the data of figure 10 up to about $t = 195$ seconds. At this point the pilot opened the bypass doors, with resulting large changes in the induction-system parameters. Area-weighted total-pressure recovery (fig. 11(b)) decreased about 5 percent and distortion increased about 6 percent. Supercritical inlet operation was obtained from $t = 195$ seconds to $t = 220$ seconds, as indicated by the cone pressures. The longitudinal acceleration of the airplane showed a decrease of $0.022g$ when the bypass area was increased, which indicates a loss in net propulsive effort of 345 pounds for the airplane weight of 15,710 pounds. The pilot reported no adverse engine operation as a result of the rapid changes. After $t = 220$ seconds the pressure recovery decreases because of the strengthening of the shock system, whereas distortion parameter remains essentially constant after $t = 240$ seconds.

A time history of the deceleration run is presented in figures 12(a) and (b). The throttle position was kept at a constant value; deceleration was obtained by extending the fuselage dive brakes. Bypass area was kept at the increased setting throughout the deceleration to provide supercritical operation. Area-weighted pressure recovery and distortion (fig. 12(a)) are sensitive to changes in the supersonic compression field. At $t = 80$ seconds supercritical operation begins, as indicated by the cone pressures, and distortion parameter shows a large increase.

Figures 13(a) and (b) present the time history of a push-down-turn maneuver performed at a Mach number of 1.7 and an altitude of 40,000 feet. The changes in Mach number are small enough so that angle of attack is the primary variable. Variations are indicated for cone pressures, distortion parameter, pressure recovery, and effective conical-compression angle.

Figure 14 presents data obtained during a ground run. Area-weighted total-pressure recovery and distortion parameter are plotted against m/m^* . During the test, auxiliary air was provided to the engine compartment through the aspirator doors. Area-weighted total-pressure recovery shows the characteristic decrease of a sharp-lip inlet as m/m^* increases (ref. 8) and reaches a value of 88 percent, with a distortion parameter of about 10 percent at maximum engine demand.

DISCUSSION

Angle-of-Attack Effects

The distortion and total-pressure-recovery data of figure 13(a) and additional similar data are plotted in figure 15(a) as a function of angle of attack. The data were selected to include all the shock configurations encountered during the investigation. Also plotted are the local total-pressure recoveries obtained near the middle of the rakes of the left-hand-compressor face. The area-weighted total-pressure recovery increases only slightly as angle of attack is increased from the lowest test limits for Mach numbers of 0.95, 1.14, and 1.35. Peak recovery is reached at angles of attack of from 6° to 7° . The data for a Mach number of 1.70 show larger effects. Thus, recovery decreased from about 91 percent to about 88 percent as angle of attack increased from 3° to 7° . Distortion parameter is unaffected by angle of attack at Mach numbers of 1.14 and 1.35. Only a slight increase is apparent for a Mach number of 0.95 as angle of attack is increased above 4° . For a Mach number of 1.70 distortion shows a sharp decrease from about 19 percent to about 15 percent as angle of attack increased above 2° .

Local total-pressure recovery H_2/H_0 of the left-hand-compressor face shows significant changes as angle of attack is increased (fig. 15(a)). For Mach numbers of 0.95, 1.14, and 1.35 the rake at the 3 o'clock position is relatively unaffected by angle of attack. The 1 o'clock rake shows an increase in recovery, whereas the 5 o'clock rake shows a decrease as angle of attack is increased. For a Mach number of 1.70 these trends are considerably altered. The 3 o'clock rake shows considerable angle-of-attack sensitivity, as indicated by the sharp decrease above an angle of attack of 2° . The 5 o'clock rake is unaffected by angle-of-attack variations and remains at a low recovery. The 1 o'clock rake recovery increases as indicated for the lower Mach numbers.

The variation of the effective conical-compression angle with angle of attack is presented in figure 15(b) for the data at $M = 1.70$. The

effective conical-compression angle decreases from about 25° to 22° as angle of attack increases above 1° .

Mach Number, Altitude, and Bypass Effects

The data of figures 10 to 12 are compared in figure 16 plotted as a function of Mach number; also included is the effective conical-compression angle for the 26,000-foot and 40,000-foot data. Trim angle-of-attack changes are noted for the several altitudes. These changes are considered to be minor compared to the Mach number, altitude, and bypass effects. A comparison of these data for identical bypass positions at trim angle of attack shows a slightly higher area-weighted total-pressure recovery H_{de}/H_0 for the 26,000-foot data up to sonic Mach number than for the 40,000-foot data. Distortion parameter D is lower than for the 40,000-foot data. The 26,000-foot pressure recovery drops sharply near sonic speed, whereas the 40,000-foot data show only a slight loss. Pressure recovery for the 40,000-foot data is about $1\frac{1}{2}$ percent higher than for the 26,000-foot data up to a Mach number of about 1.55 where the bypass configuration is changed. Distortion parameter decreases at about the same rate for both sets of data beyond a Mach number of about 1.2. The data at 26,000 feet showed about $2\frac{1}{2}$ percent less distortion for this Mach number region, and the effective cone angle reached a maximum for both sets of data for the Mach number range from about 1.45 to about 1.6. A pressure recovery of about 95 percent and a distortion of 15 percent were noted for the 40,000-foot data at a Mach number of about 1.55.

For the Mach number range from 1.55 to 1.65 and from 1.90 to 2.05 at trim angle of attack the 40,000-foot and 55,000-foot pressure-recovery data are essentially the same. A value of about 81 percent was noted for a Mach number of 2.05 for both sets of data. Good agreement is shown with the data of reference 9. The cone pressures indicate very similar terminal-shock-wave configurations (figs. 11(b) and 12(b)) for these Mach number ranges. A distortion parameter of 33 percent was obtained for the 55,000-foot data at a Mach number of approximately 1.24 during supercritical operation. For the Mach number range from 1.90 to 1.65 the normal shock is further downstream for the 55,000-foot data than for the 40,000-foot data (figs. 11(b) and 12(b)), with the consequent decrease in recovery and increase in distortion shown.

In figure 17 the local total-pressure recovery of the left-hand-compressor face is plotted as a function of Mach number. In figure 17(a) the 26,000-foot data indicate higher recovery for the 5 o'clock rake position than is shown by the 40,000-foot data for subsonic Mach

numbers. The 3 o'clock rake shows the same recovery and the 1 o'clock data show slightly lower recovery for this speed range. At sonic speed a much larger decrement in pressure recovery is shown for the 26,000-foot data than for the 40,000-foot data. From sonic speed to the test limits, only a slight change is noted for the 3 o'clock rake recovery, whereas the 5 o'clock rake recovery shows a steady increase. The recovery for the 3 o'clock rake at 40,000 feet is higher than the calculated recovery through the inferred shock system above $M = 1.1$. This result indicates shock-boundary-layer interaction in the form of a lambda shock and agrees with the data of reference 4. The 1 o'clock rake recovery shows the largest sensitivity to Mach number. The downward trend shown for subsonic speeds is reversed at about $M = 1.10$. A steady increase is then noted until the Mach number for shock attachment ($M = 1.35$ to 1.40) is reached. A large increase in pressure recovery occurs at this point as a result of the higher compression efficiency of the conical shock. At about $M = 1.5$ the terminal normal shock is formed and reduces the slope of the recovery curve for both the 26,000-foot and 40,000-foot data.

A comparison of the 40,000-foot and 55,000-foot data shows good agreement for the 1 o'clock and 3 o'clock rakes for the Mach number range from 1.90 to 2.05 (fig. 17(b)). Good agreement is also noted for the 5 o'clock rake at Mach numbers in excess of 2.0 and for the 3 o'clock rake at Mach numbers from 1.6 to 1.7. These regions correspond to very similar shock-wave configurations for the two altitudes (figs. 11(b) and 12(b)). Both sets of data show marked changes in local recovery due to the shock-system changes. Thus, the changes in local recovery for the Mach number range from $M = 1.6$ to $M = 1.8$ are a result of the terminal-shock movement (figs. 11(b) and 12(b)). The effect of conical-shock attachment is indicated at about $M = 1.4$ for the 55,000-foot data at the three rake positions.

Figure 18 presents plots of local total-pressure recovery for the entire compressor face at 26,000 feet for no-shock ($M = 0.90$), single normal-shock ($M = 1.17$), and two-shock compression ($M = 1.58$). The plot for $M = 0.90$ indicates symmetry about a horizontal and vertical center line, with the highest recovery obtained at the 3 o'clock and 9 o'clock positions. The foregoing distortion remains essentially unchanged for $M = 1.17$. For $M = 1.58$ with an attached conical system, however, only vertical center-line symmetry is present. Highest recovery is obtained at the 3 o'clock and 9 o'clock positions, with lowest recovery at the bottom of the duct. Local recovery exhibited symmetry about the vertical center line of the engine face for all data presented in this paper.

In figure 19 cone-pressure profiles are presented for several Mach numbers and both bypass positions. For the same Mach number all test

data showed essentially the same cone-pressure profiles. With the smaller bypass area (fig. 19(a)) plots are presented for no-shock ($M = 0.9$), single normal-shock ($M = 1.2$), and two-shock compression ($M = 1.5$). Shock formation is indicated for $M = 1.2$ and $M = 1.5$ between orifices S_2 and O_1 . For $M = 0.9$ and $M = 1.2$, expansion along the cone is evident from orifices O_2 to O_3 for both sets of data; a slightly greater amount is noted for the 40,000-foot data at $M = 1.2$. Terminal-shock formation between orifices O_2 and O_3 is indicated for the data at $M = 1.5$. Shock-boundary-layer interaction is indicated for the 40,000-foot data because of the smaller pressure increment between orifices O_2 and O_3 . The advantage of the boundary-layer-removal slot is apparent from the pressure increment noted between orifices O_4 and O_5 .

For the larger bypass area (fig. 19(b)) all data show two-shock compression. For $M = 1.6$ the terminal shock is between orifices O_4 and O_5 and for $M = 1.8$ is between orifices O_3 and O_4 . For $M = 2.0$ the terminal-shock system appears to affect both orifice O_3 and O_4 . This result indicates a lambda shock due to shock-boundary-layer interaction. Additional shock-boundary-layer effects are indicated for the data at $M = 1.6$ and $M = 1.8$. Thus, the pressure-profile curves deviate downstream of the shock location. The effect of the boundary-layer-removal slot on the compression process between O_4 and O_5 is again evident.

CONCLUSIONS

Flight tests of a twin-duct induction system over a Mach number range from about 0.78 to about 2.07 during quasi-steady operation indicated the following conclusions:

1. Over the Mach number range from about 1.05 to about 1.55 the 40,000-foot data exhibited about a $1\frac{1}{2}$ percent higher recovery than did the 26,000-foot data for very similar subcritical shock-wave configuration and identical bypass configuration at trim angle of attack. The 26,000-foot data showed significantly lower distortion, however. A pressure recovery of about 95 percent and a distortion parameter of 15 percent were noted for the 40,000-foot data at a Mach number of about 1.55.

2. The 40,000-foot data and 55,000-foot data showed essentially the same recovery for very similar shock-wave configuration and the increased bypass configuration at trim angle of attack. A value of about 81 percent was noted for a Mach number of 2.05 for both sets of data. A distortion parameter of 33 percent was obtained for the 55,000-foot data at a Mach number of approximately 1.24 during supercritical operation.

3. At a Mach number of 1.70, area-weighted pressure recovery decreased from about 91 percent to about 88 percent as angle of attack increased from 3° to 7° , whereas the distortion parameter decreased from 19 percent to 15 percent as angle of attack increased above 2° . Angle of attack produced only slight effects at lower Mach numbers.

4. Local recovery exhibited symmetry about the vertical center line of the engine face for all data. Highest recovery was obtained at the 3 o'clock and 9 o'clock rake positions, with lowest recovery obtained at the bottom of the duct during level flight.

5. For the same Mach number all test data showed essentially the same cone-pressure profiles. Shock-boundary-layer interaction along the cone surface occurred for the 40,000-foot data and the 55,000-foot data for Mach numbers of 1.5 and greater. This result affected the cone-surface pressure distribution.

6. During ground-run operation, a recovery of about 88 percent and a distortion parameter of about 10 percent were obtained for maximum engine demand.

Flight Research Center,
National Aeronautics and Space Administration,
Edwards, Calif., February 5, 1960.

REFERENCES

1. Nugent, Jack: Interaction of Nonsteady Twin-Inlet Flow and Airplane Directional Motions at a Mach Number of Approximately 1.9. NASA TM X-54, 1959.
2. Davis, Wallace F., and Scherrer, Richard: Aerodynamic Principles for the Design of Jet-Engine Induction Systems. NACA RM A55F16, 1956.
3. Aircraft Gas Turbine Division: Estimated Minimum Performance-General Electric J79 Phase I Turbojet Engine. Bulletin No. R56AGT129, General Electric Co., Sept. 15, 1956.
4. Stitt, Leonard E., McKeivitt, Frank X., and Smith, Albert B.: Effect of Throat Bleed on the Supersonic Performance of a Half-Conical Side-Inlet System. NACA RM E55J07, 1956.
5. Anderson, Warren E., and Perkins, Edward W.: Effects of Unsymmetrical Air-Flow Characteristics of Twin-Intake Air-Induction Systems on Airplane Static Stability at Supersonic Speeds. NASA TM X-94, 1959.
6. Dailey, Charles L., and Wood, Frank C.: Computation Curves for Compressible Fluid Problems. John Wiley & Sons, Inc., 1949.
7. Hermann, Rudolf: Supersonic Inlet Diffusers and Introduction to Internal Aerodynamics. Minneapolis Honeywell Regulator Co., 1956.
8. Fradenburgh, Evan A., and Wyatt, DeMarquis D.: Theoretical Performance Characteristics of Sharp-Lip Inlets at Subsonic Speeds. NACA Rep. 1193, 1954. (Supersedes NACA TN 3004.)
9. Stitt, Leonard E., Cubbison, Robert W., and Flaherty, Richard J.: Performance of Several Half-Conical Side Inlets at Supersonic and Subsonic Speeds. NACA RM E55J10a, 1956.

TABLE I.- GEOMETRIC CHARACTERISTICS OF THE AIRPLANE

Wing:

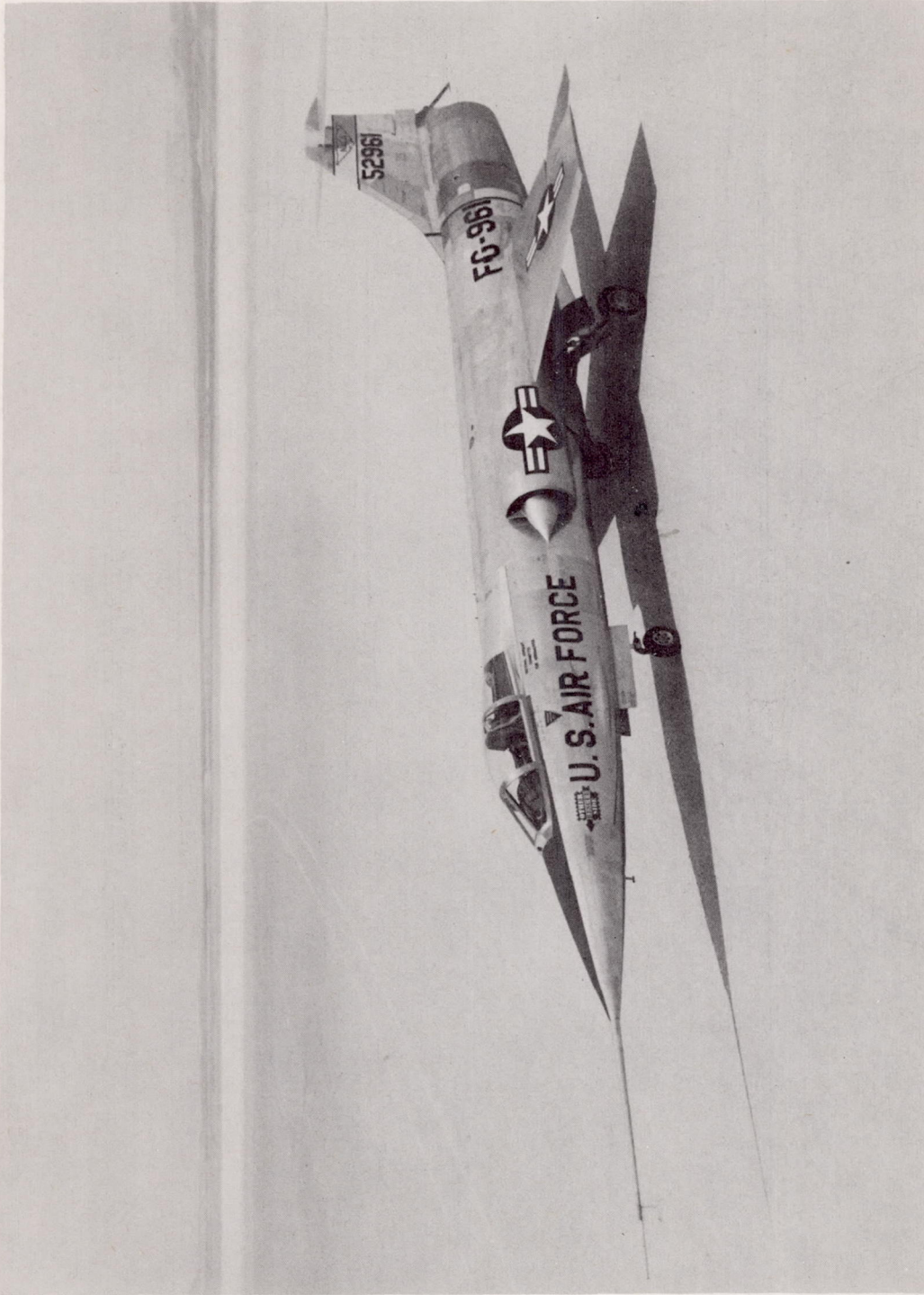
Airfoil section	Modified biconvex
Area, sq ft	196.1
Span, ft	21.94
Mean aerodynamic chord, ft	9.55
Root chord, ft	12.98
Tip chord, ft	4.89
Aspect ratio	2.45
Taper ratio	0.378
Sweep at 25-percent chord, deg	18.1
Sweep at the leading edge, deg	27.3
Incidence, deg	0
Dihedral, deg	-10.0
Airfoil thickness ratio	0.0336
Leading-edge flaps (per side) -	
Area, sq ft	8.50
Mean chord, ft	1.012
Deflection limit, deg	-30
Type	Plain
Trailing-edge flaps (per side) -	
Area, sq ft	11.55
Mean chord, ft	2.52
Deflection limit, deg	45
Type	Plain
Ailerons (per side) -	
Area, sq ft	4.73
Mean chord, ft	1.716
Span, ft	2.75
Deflection, deg	±15

Tail:

Horizontal tail -	
Airfoil section	Modified biconvex
Area, sq ft	48.2
Mean aerodynamic chord, ft	4.415
Span, ft	11.92
Root chord, ft	6.16
Tip chord, ft	1.917
Aspect ratio	2.95
Taper ratio	0.311
Root thickness ratio	0.0493
Tip thickness ratio	0.0261
Tail length, 25-percent wing mean aerodynamic chord to	
25-percent horizontal-tail mean aerodynamic chord, ft	18.72
Sweep at 25-percent mean aerodynamic chord, deg	10.12
Deflection limits, deg	5 to -17

TABLE I.- GEOMETRIC CHARACTERISTICS OF THE AIRPLANE - Concluded

Vertical tail -	
Airfoil section	Modified biconvex
Area, sq ft	35.1
Span, ft	5.46
Mean aerodynamic chord, ft	6.88
Aspect ratio	0.849
Taper ratio	0.371
Tail length, 25-percent wing mean aerodynamic chord to 25-percent vertical-tail mean aerodynamic chord, ft	15.13
Sweep at 25-percent mean aerodynamic chord, deg	35
Rudder -	
Area, sq ft	4.3
Span, ft	2.92
Average chord, ft	1.375
Deflection limit, deg	±25
Yaw damper -	
Area, sq ft	1
Span, ft	1
Average chord, ft	1
Deflection limit, deg	±20
Fuselage:	
Frontal area, sq ft	25
Length, ft	51.25
Fineness ratio	9.09
Dive brakes (per side):	
Area (projected frontal area at maximum deflection), sq ft	4.13
Chord, ft	2.50
Deflection limit, deg	60
Weight:	
Empty weight, lb	13,237
Total take-off weight, lb	18,233
Center-of-gravity location, percent mean aerodynamic chord -	
Empty	17.40
Take-off	5.25



E-3022

Figure 1.- Photograph of the test airplane.

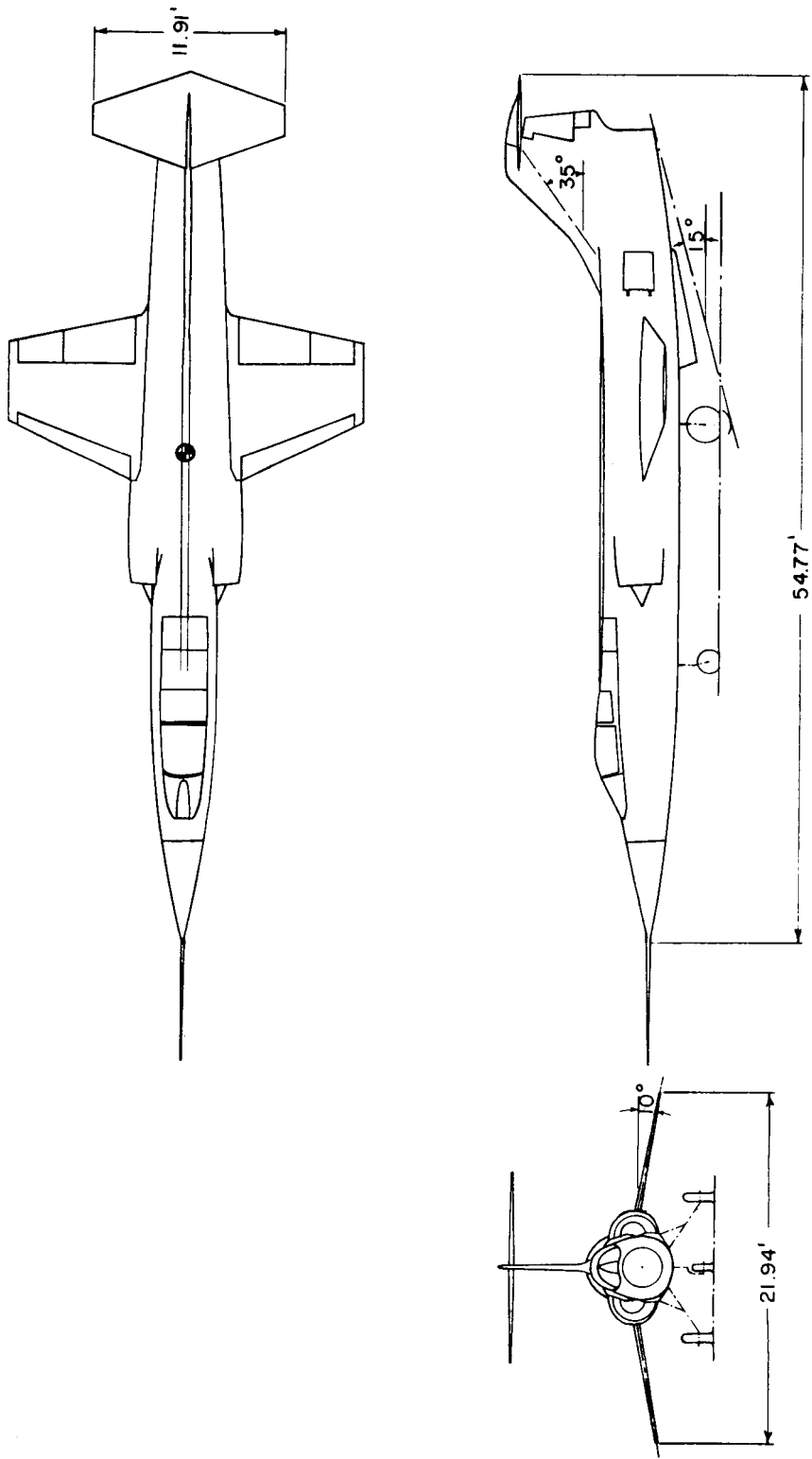


Figure 2.- Three-view drawing of the test airplane.

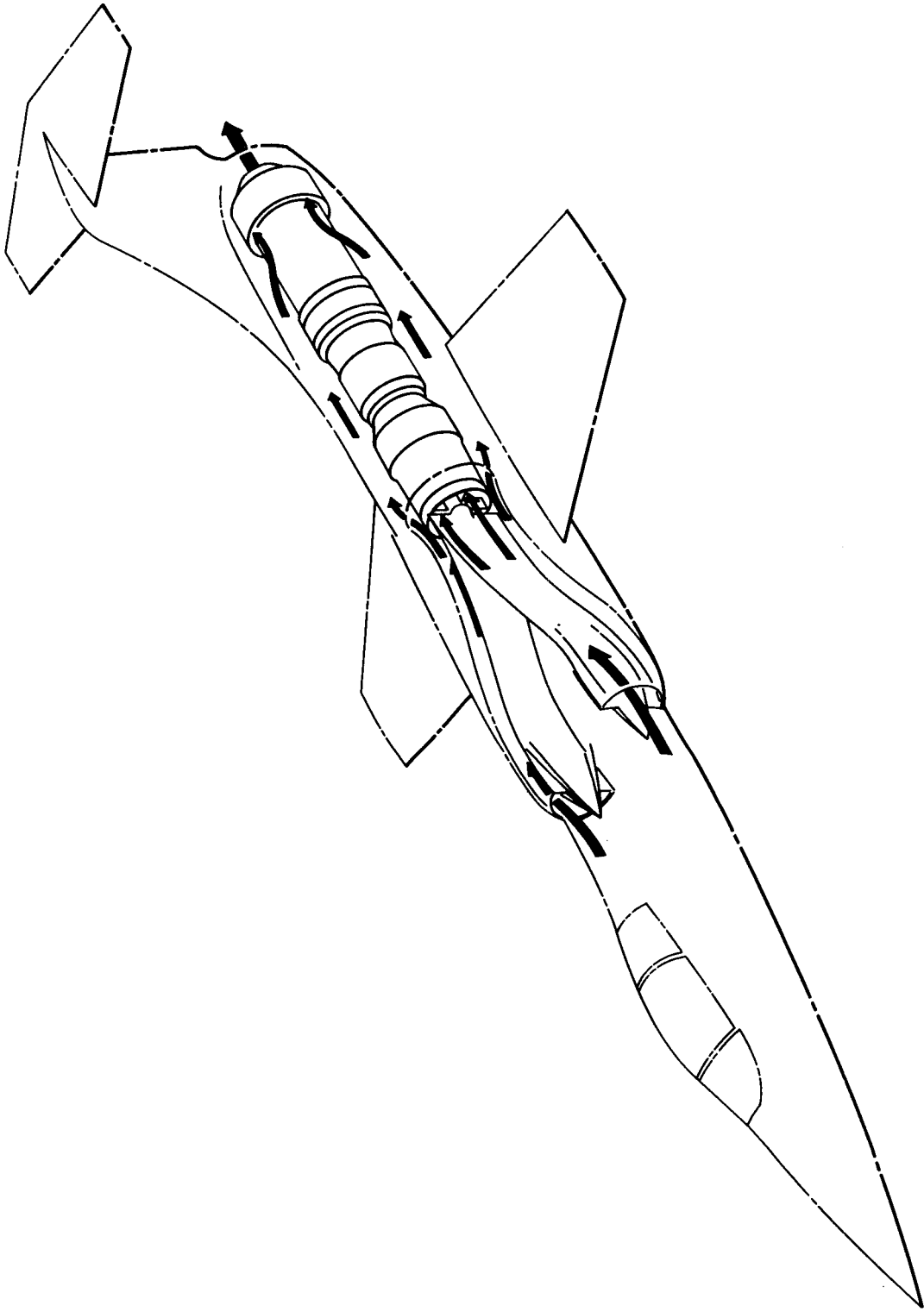
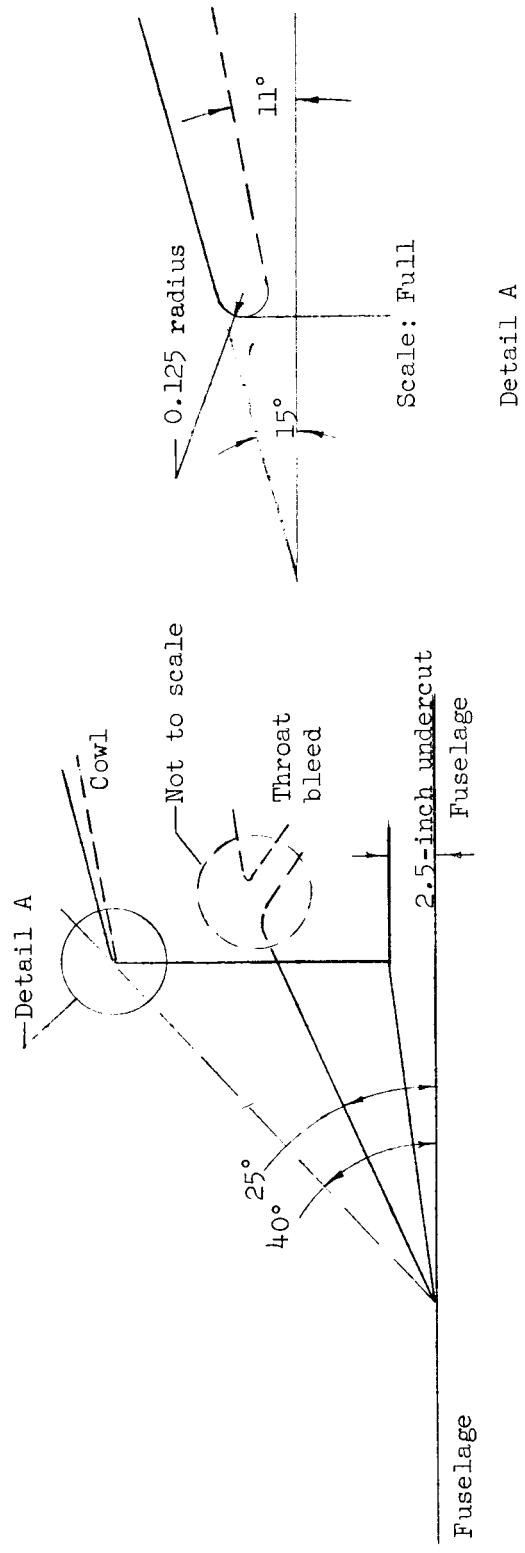


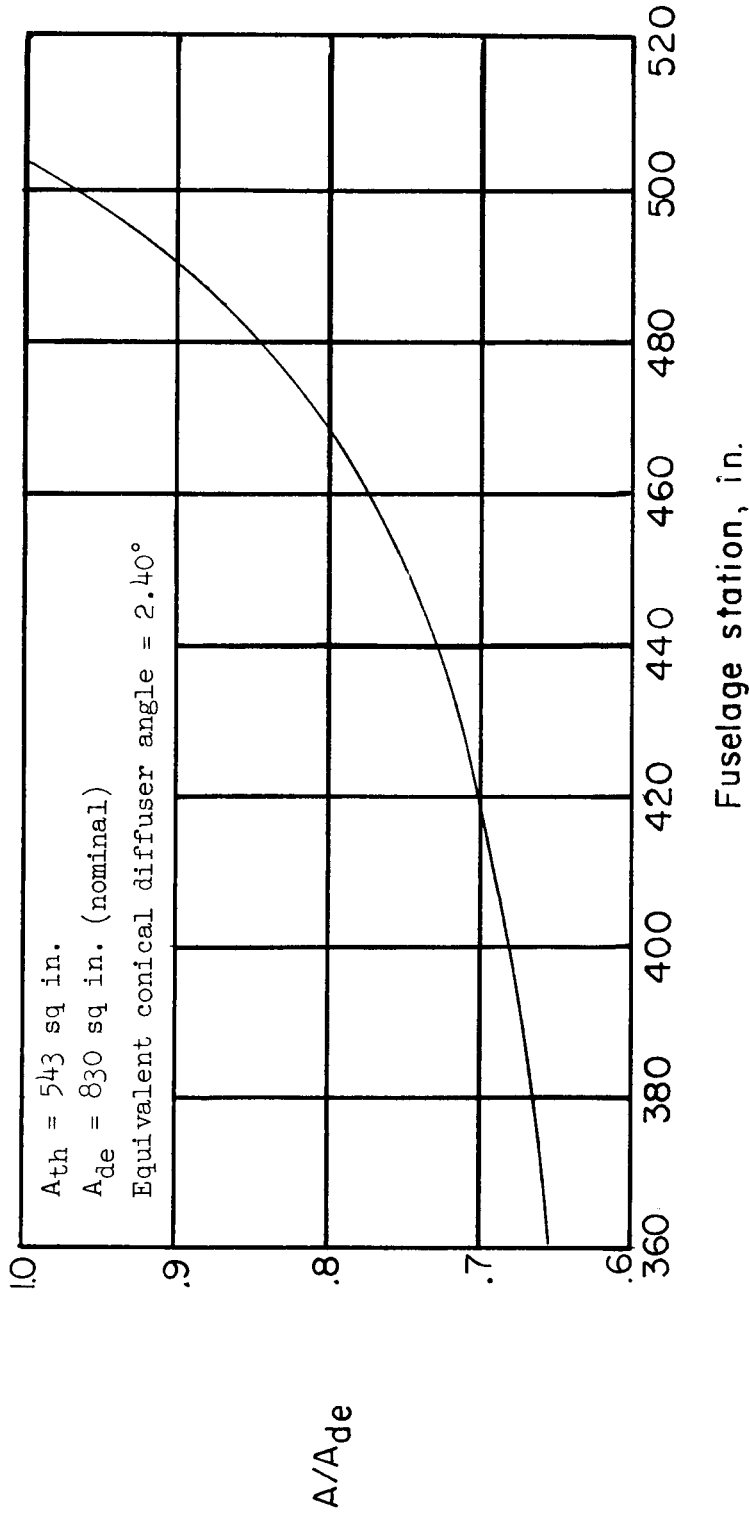
Figure 3.- Schematic drawing of internal-flow system.



Capture area - 763 sq in. (both sides)

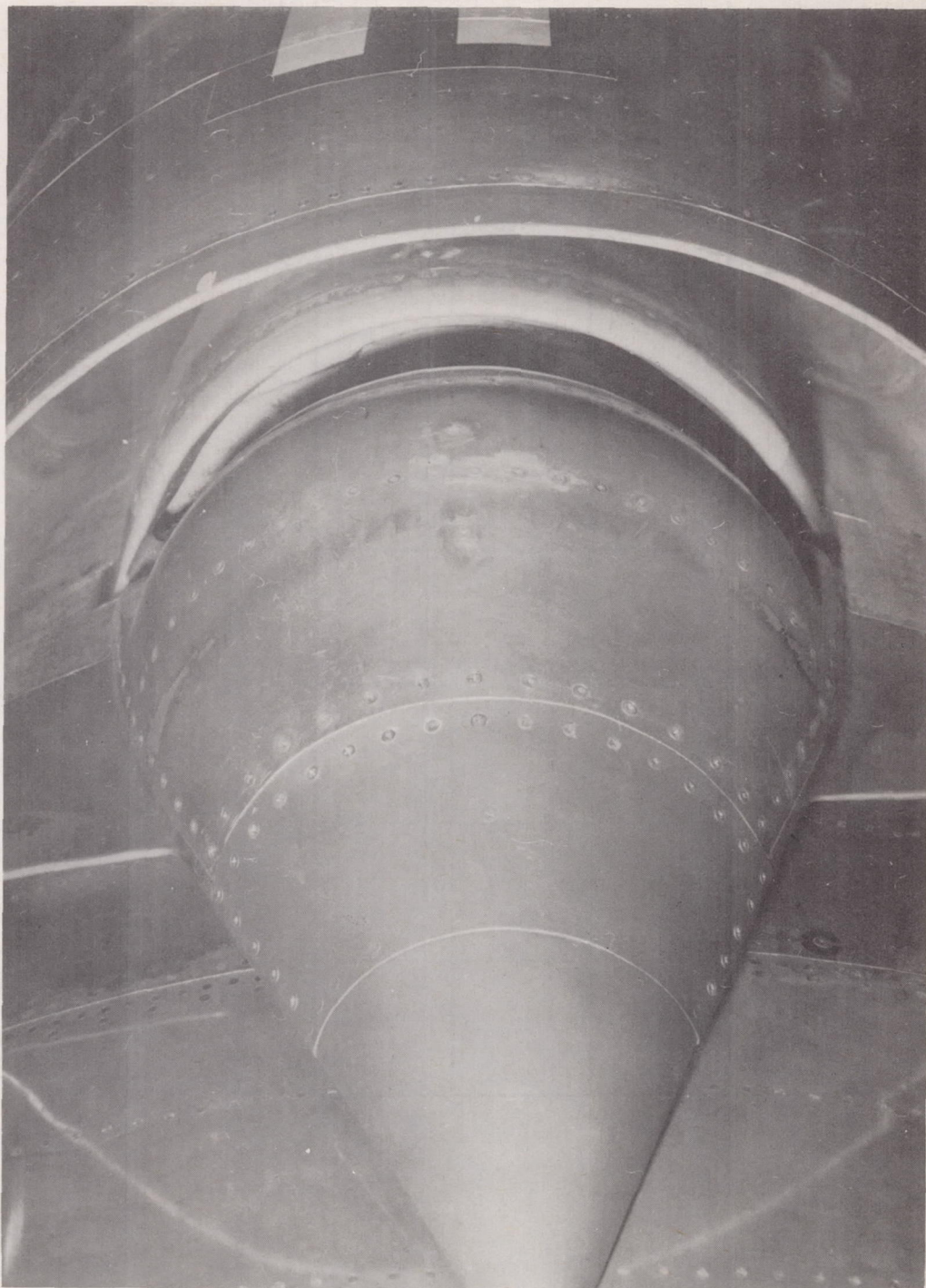
(a) Inlet details.

Figure 4.- Details of diffuser geometry.



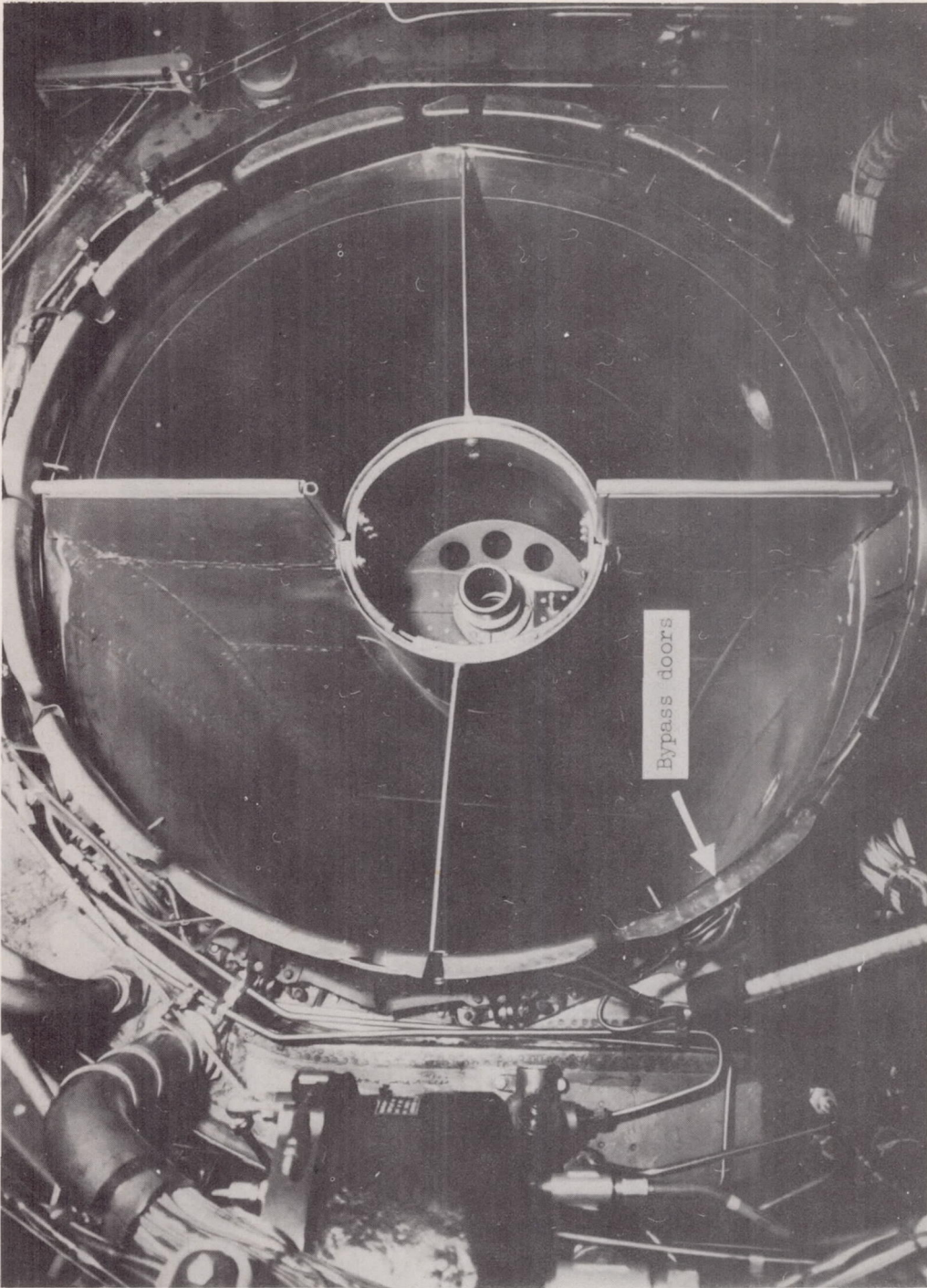
(b) Duct-area distribution.

Figure 4.- Concluded.



(a) Diffuser entrance. E-5080

Figure 5.- Photographs of diffuser.



E-3104

(b) Diffuser exit.

Figure 5.- Concluded.

CONFIDENTIAL

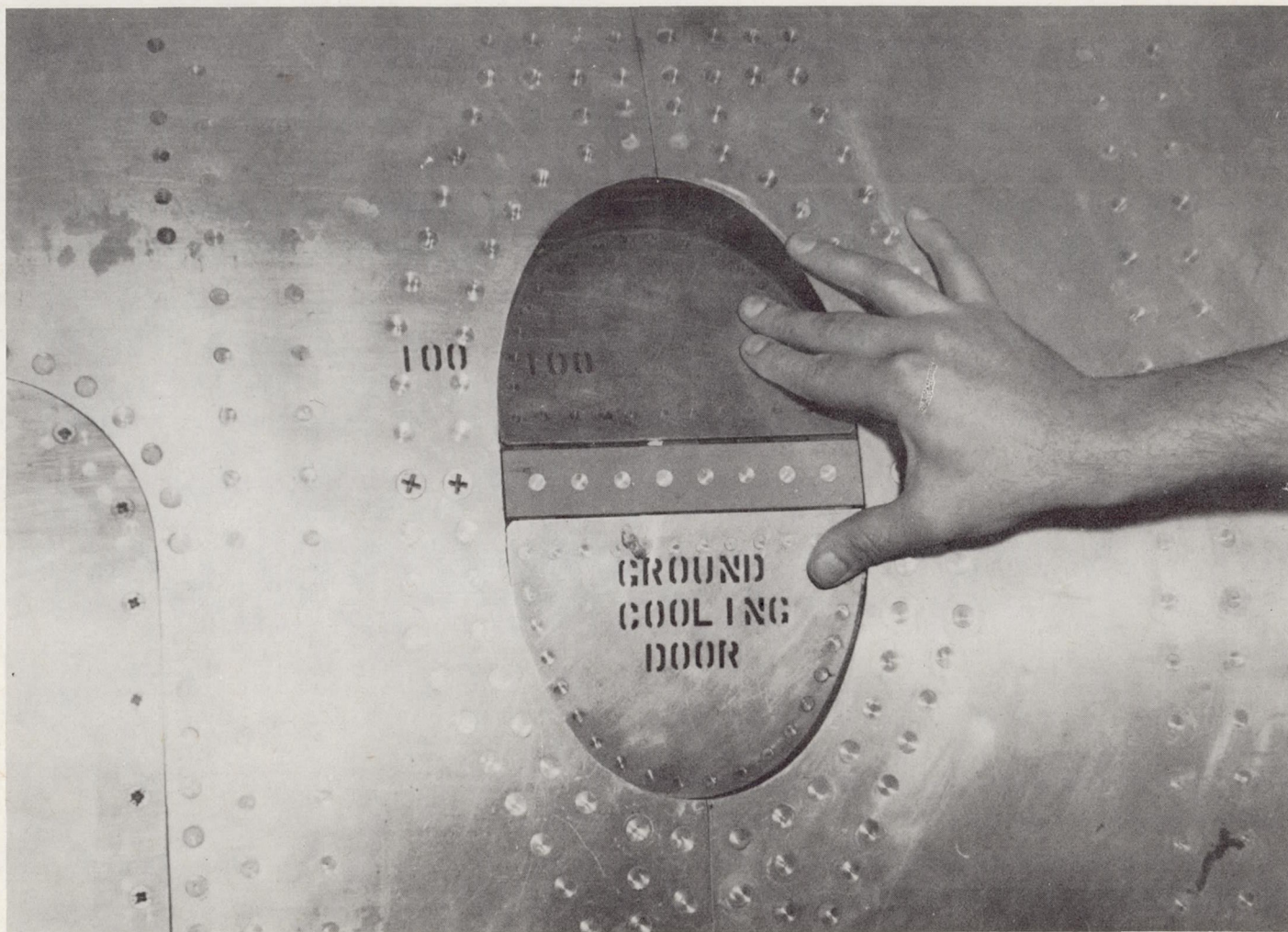


Figure 6.- Photograph of a typical aspirator door installed in the fuselage. E-5079

CONFIDENTIAL

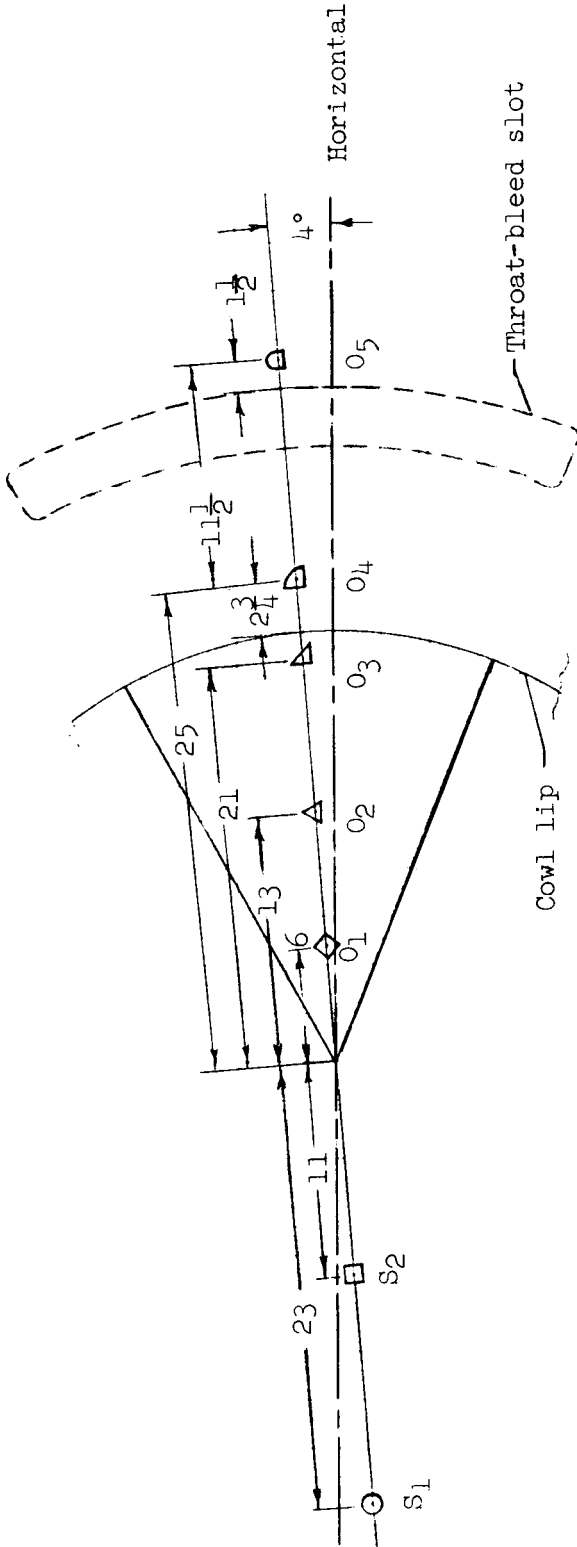


Figure 8.- Diagram of static-pressure orifices on and near the left-inlet cone. All dimensions in inches.

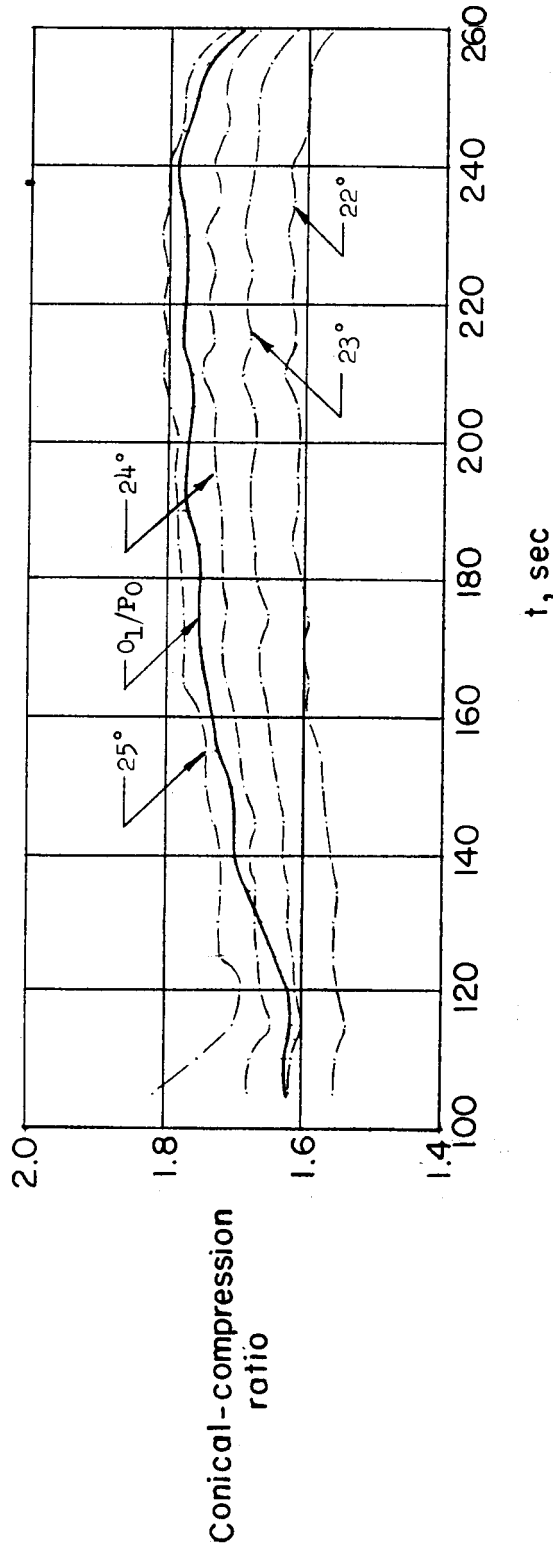
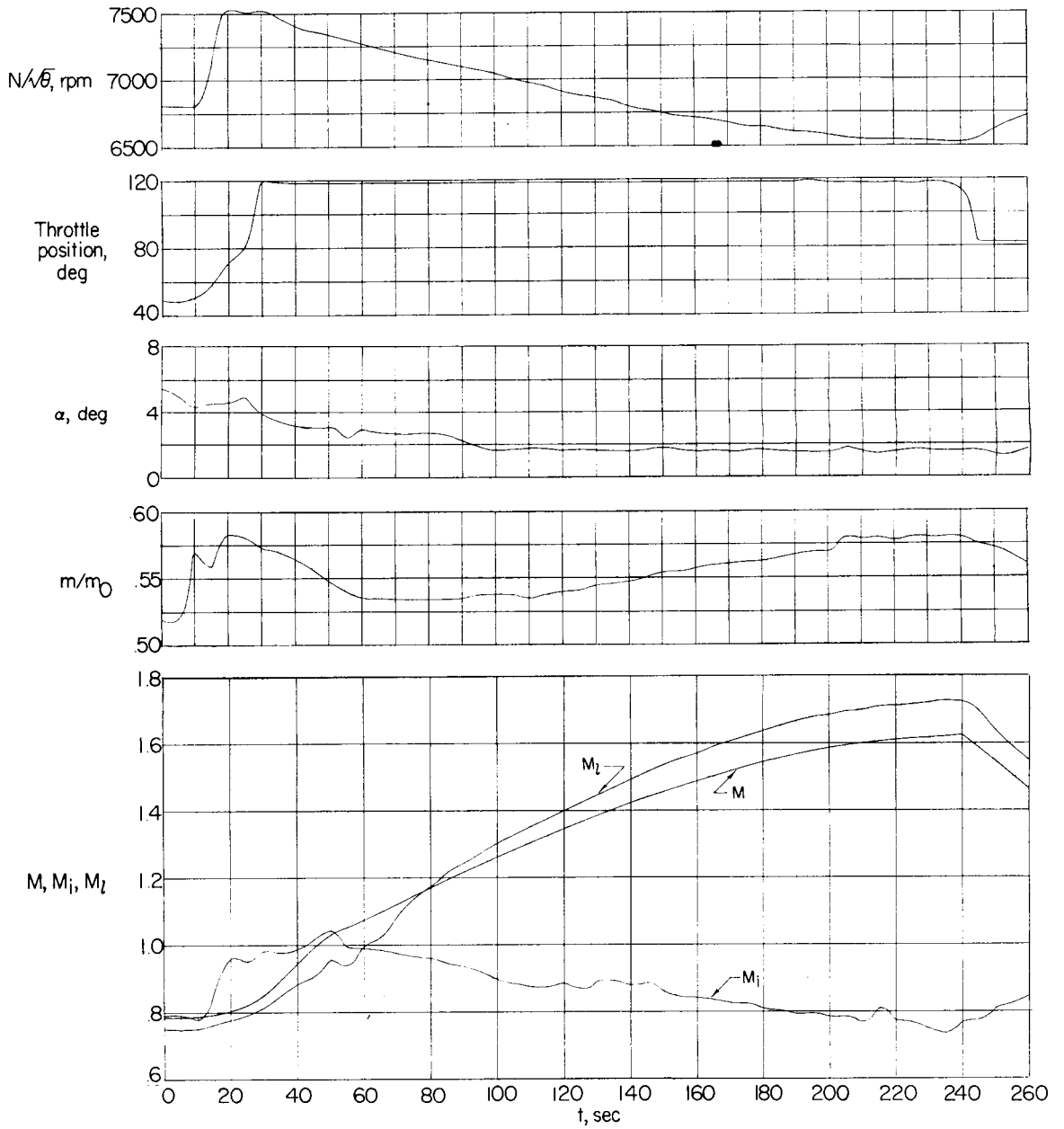
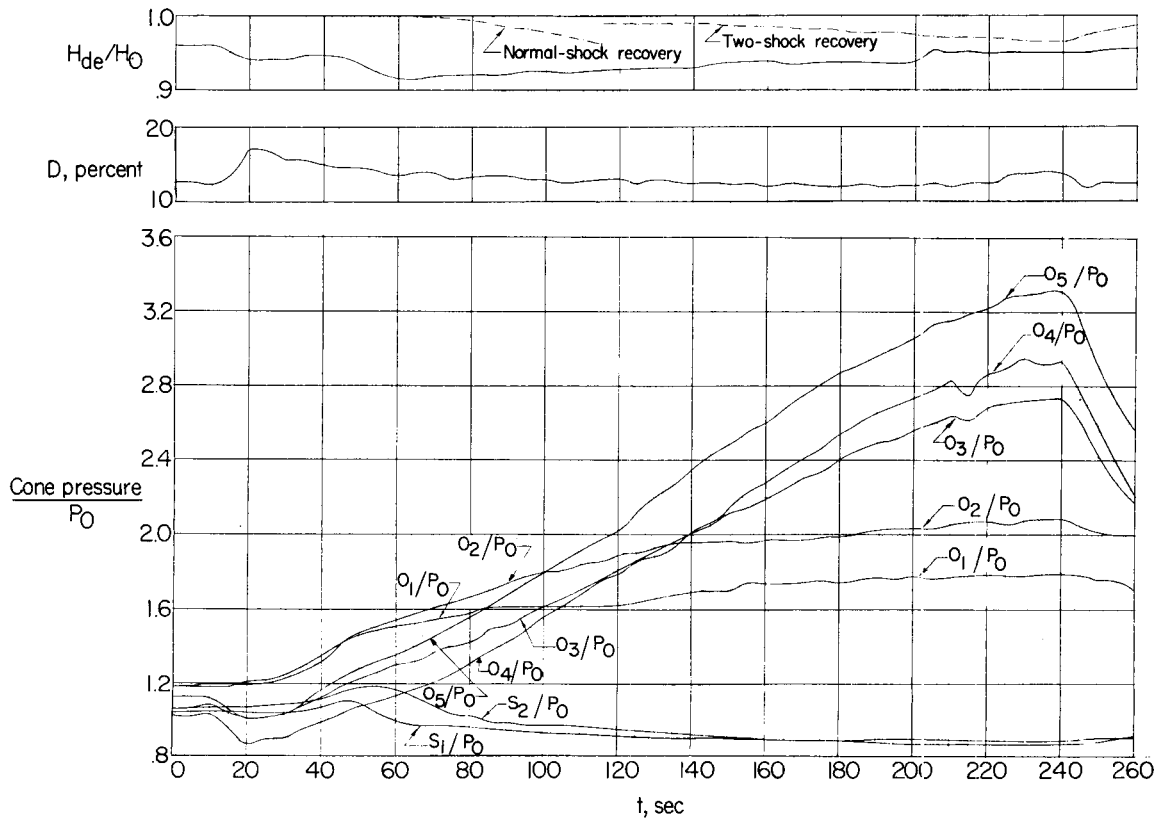


Figure 9.- Method for determining effective conical-compression angle.



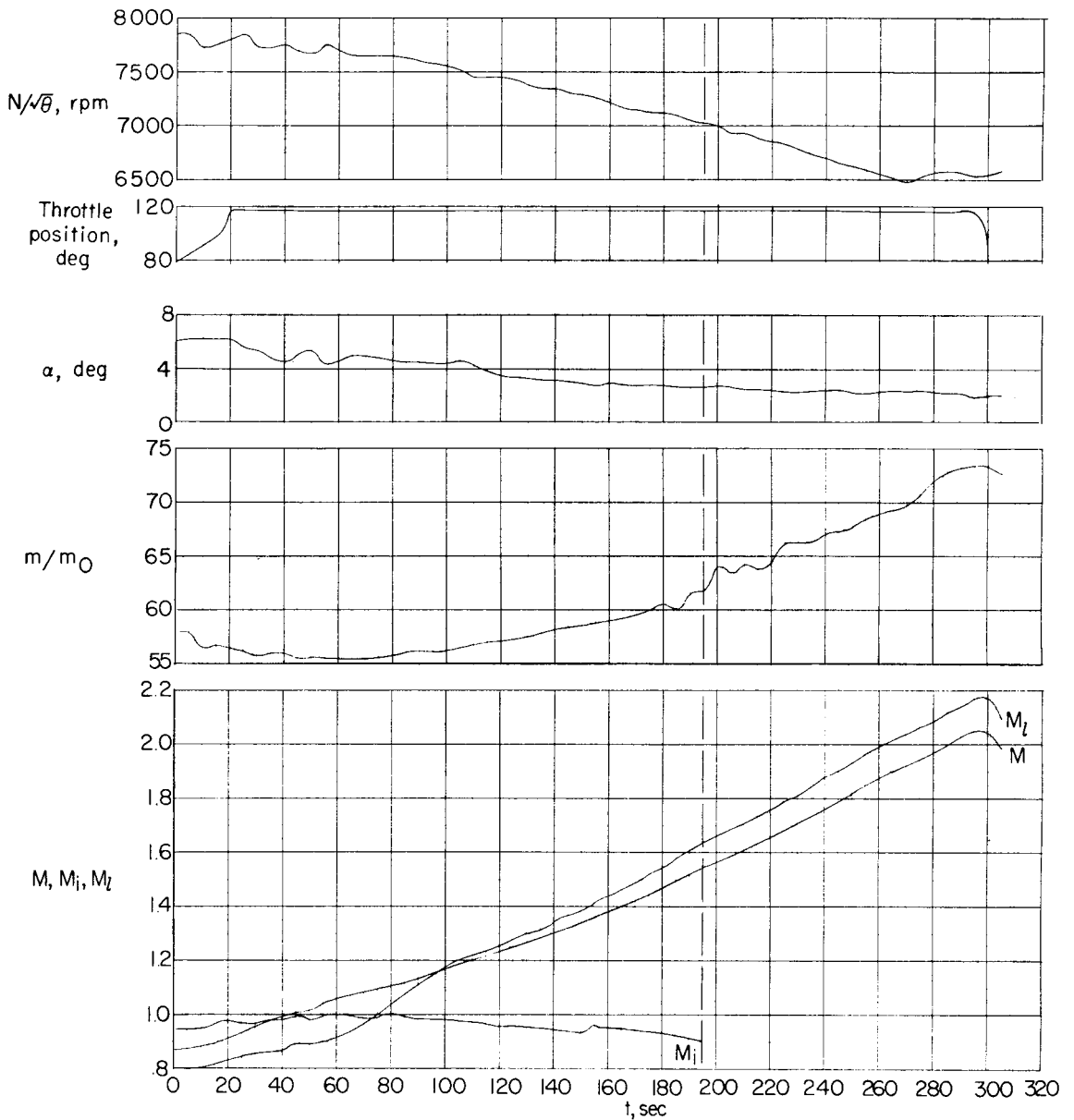
(a) Induction-system, engine, and airplane parameters.

Figure 10.- Time history of an acceleration at an altitude of 26,000 feet.



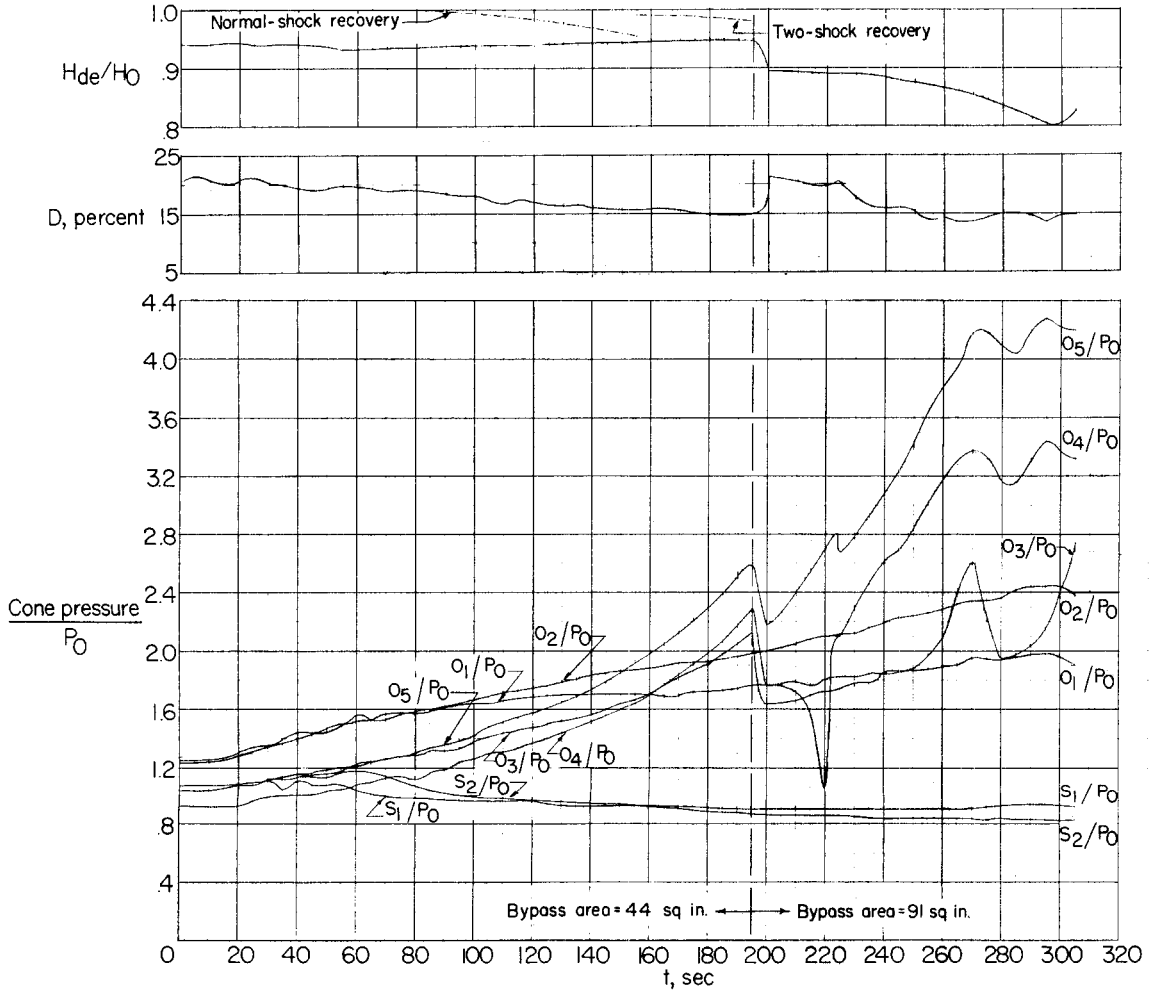
(b) Pressure recovery, distortion, and cone pressures.

Figure 10.- Concluded.



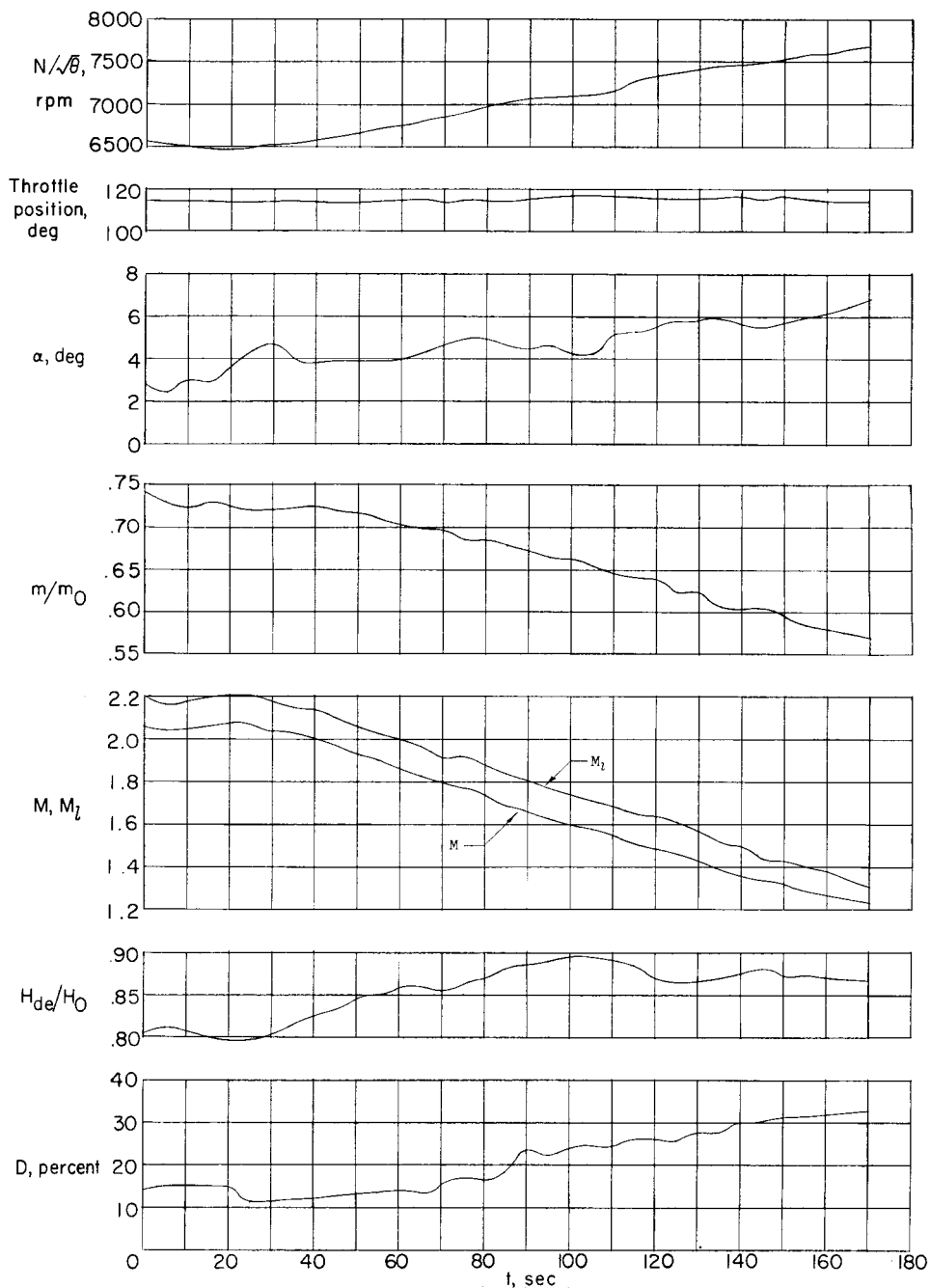
(a) Induction-system, engine, and airplane parameters.

Figure 11.- Time history of an acceleration at an altitude of 40,000 feet.



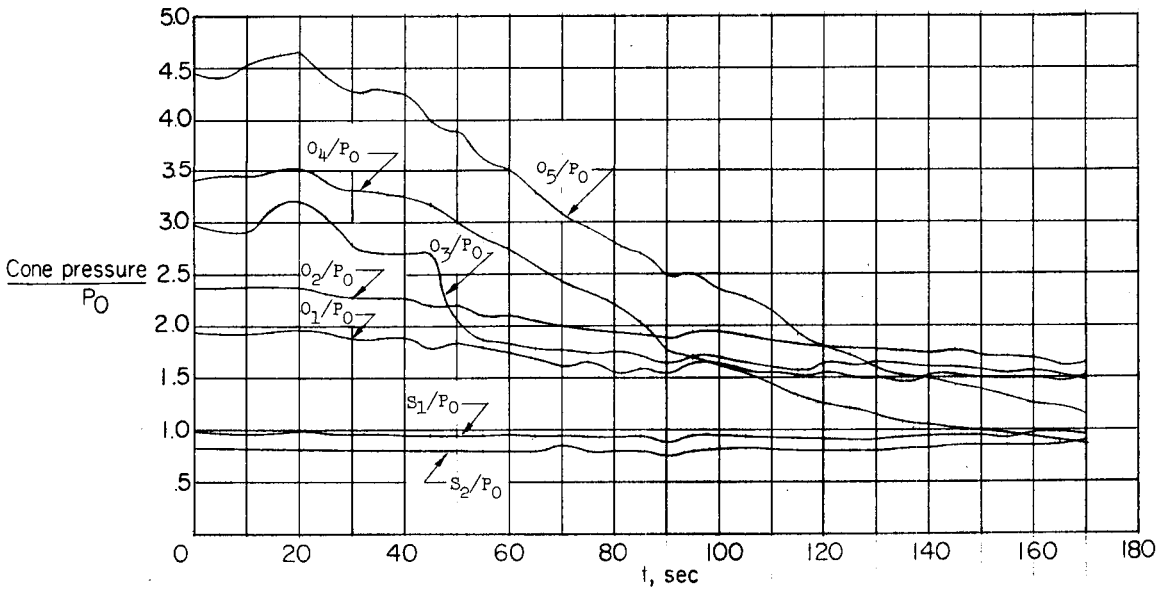
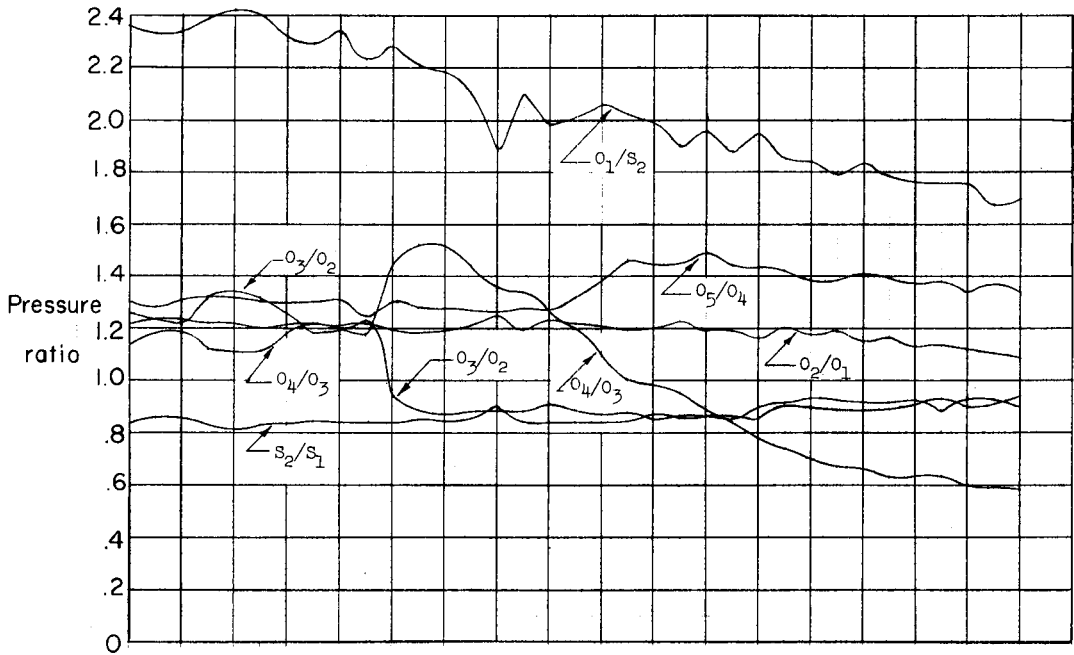
(b) Pressure recovery, distortion, and cone pressures.

Figure 11.- Concluded.



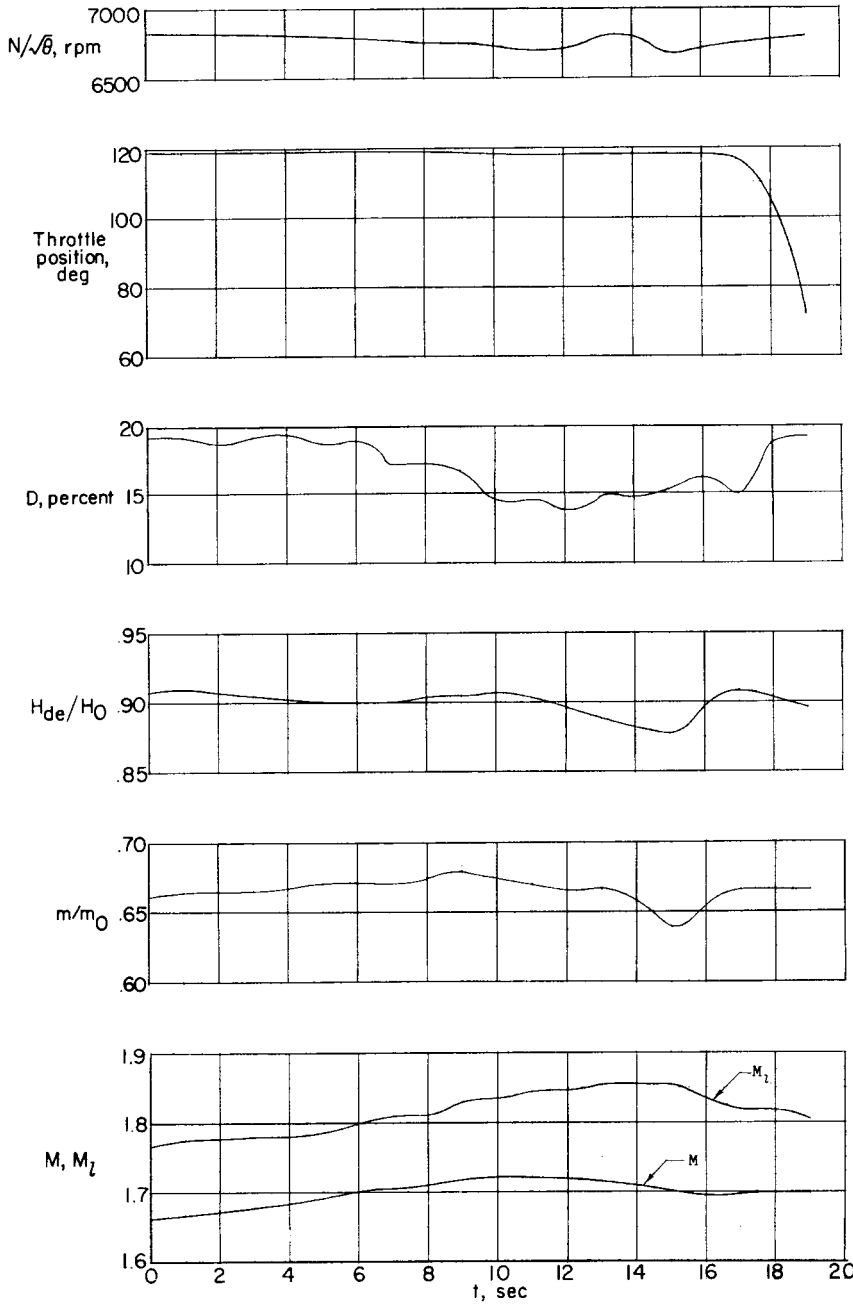
(a) Induction-system, engine, and airplane parameters.

Figure 12.- Time history of a deceleration at an altitude of 55,000 feet.



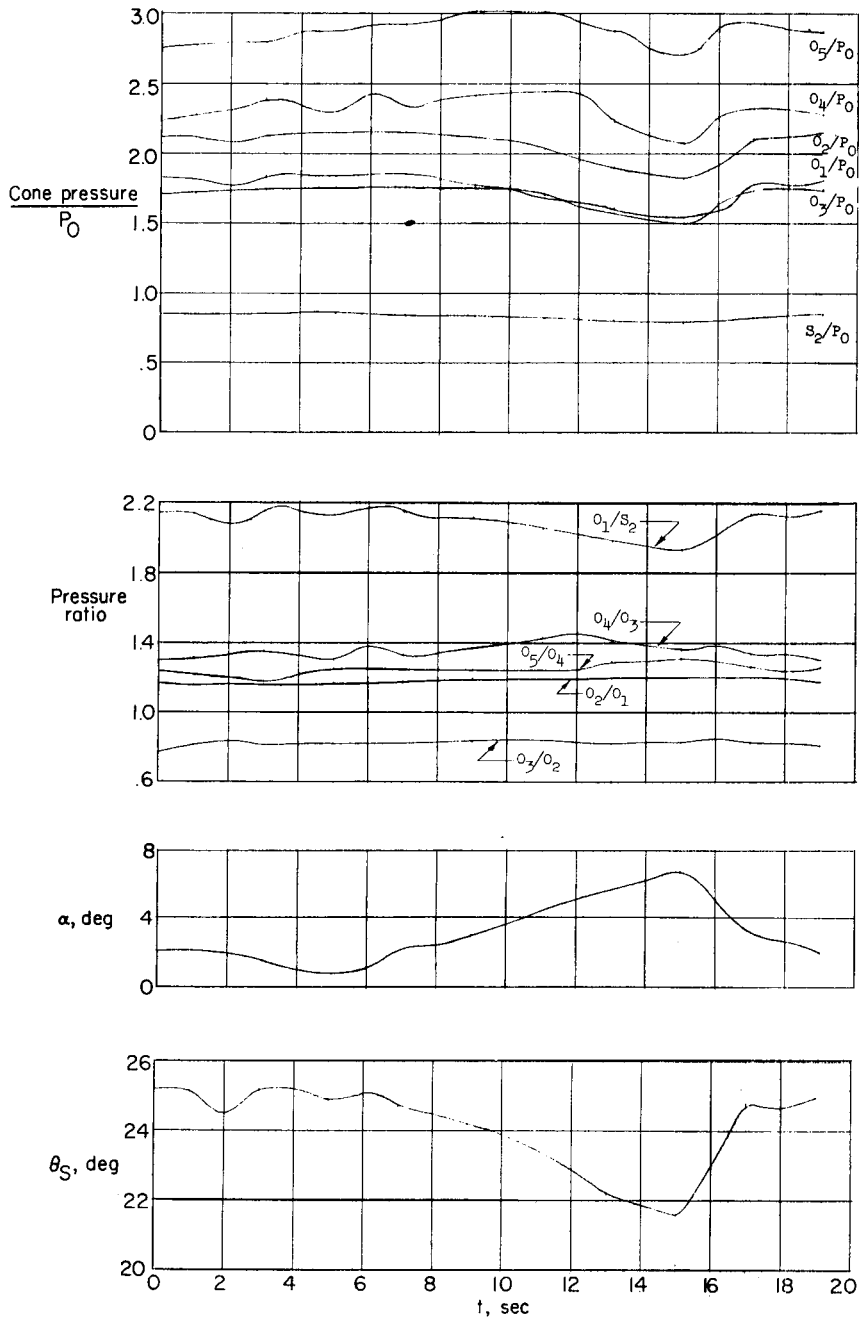
(b) Cone pressures.

Figure 12.- Concluded.



(a) Induction-system, engine, and airplane parameters.

Figure 13.- Time history of a push-down-turn maneuver at a Mach number of 1.7 and an altitude of 40,000 feet.



(b) Cone pressures, angle of attack, and effective conical-compression angle.

Figure 13.- Concluded.

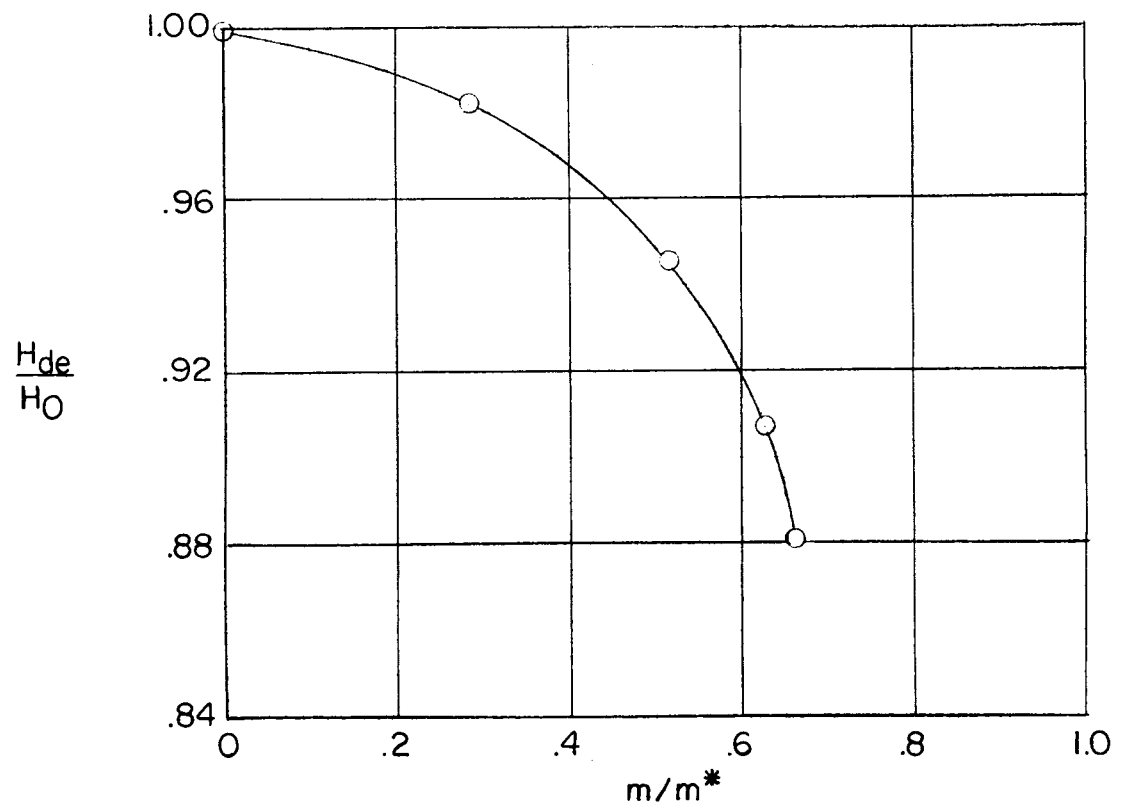
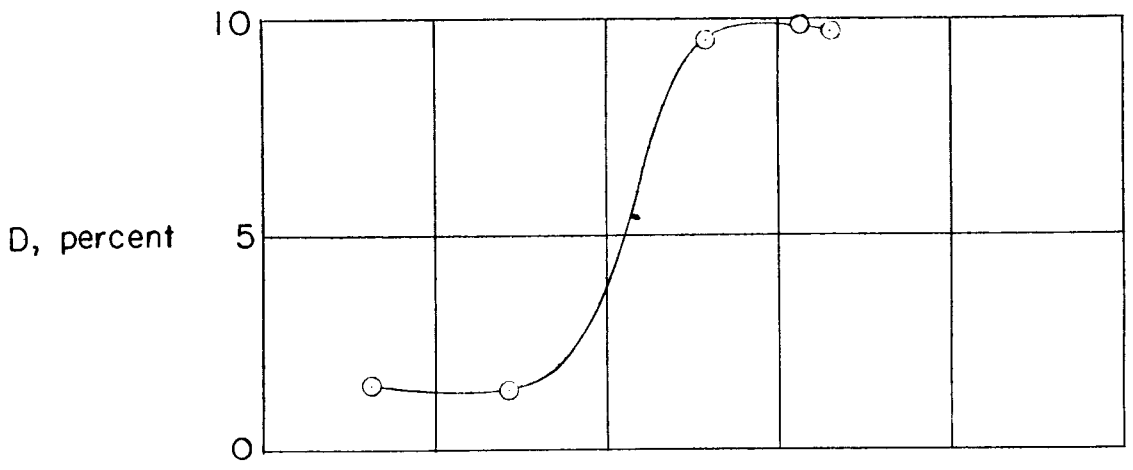
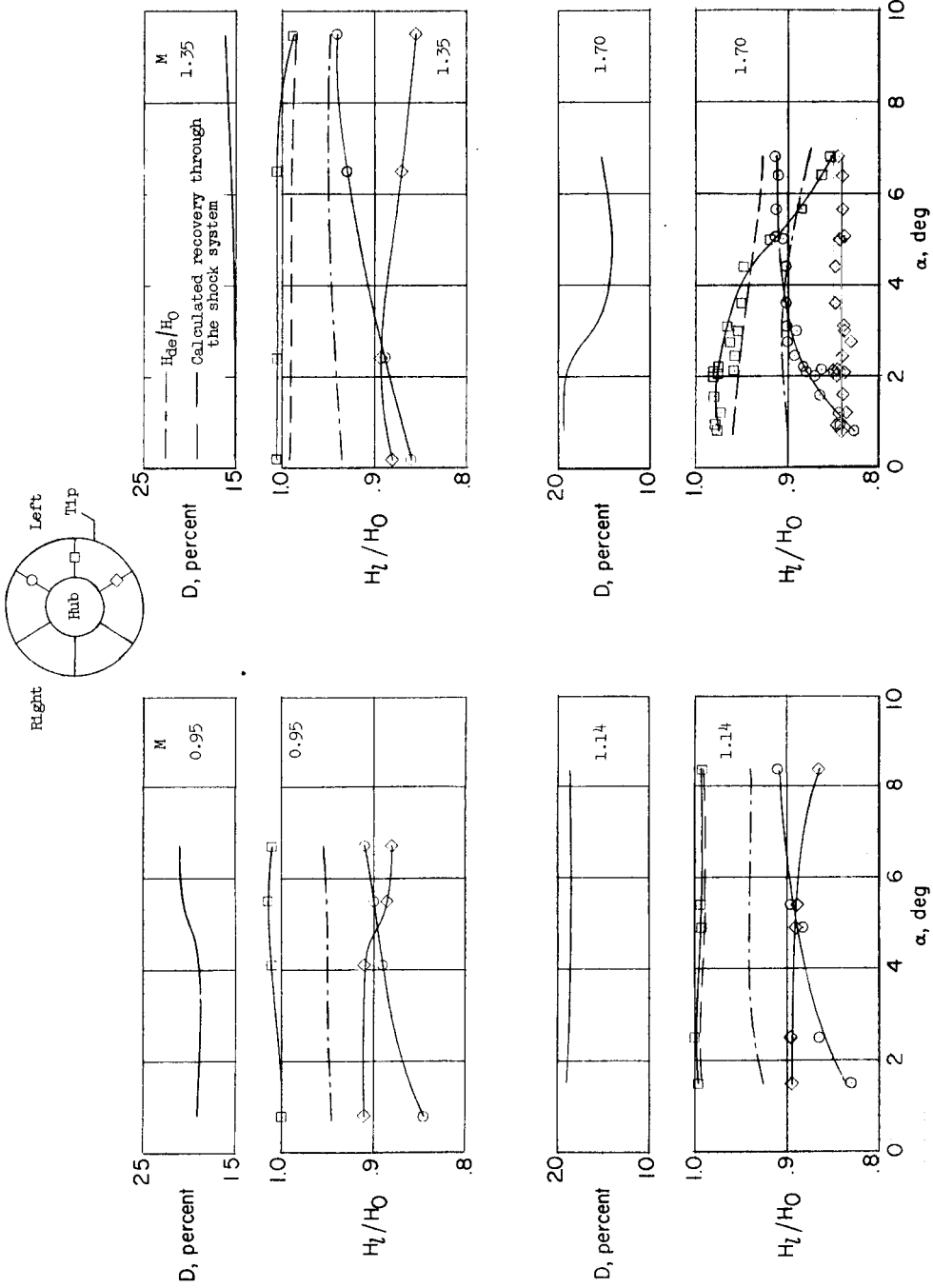
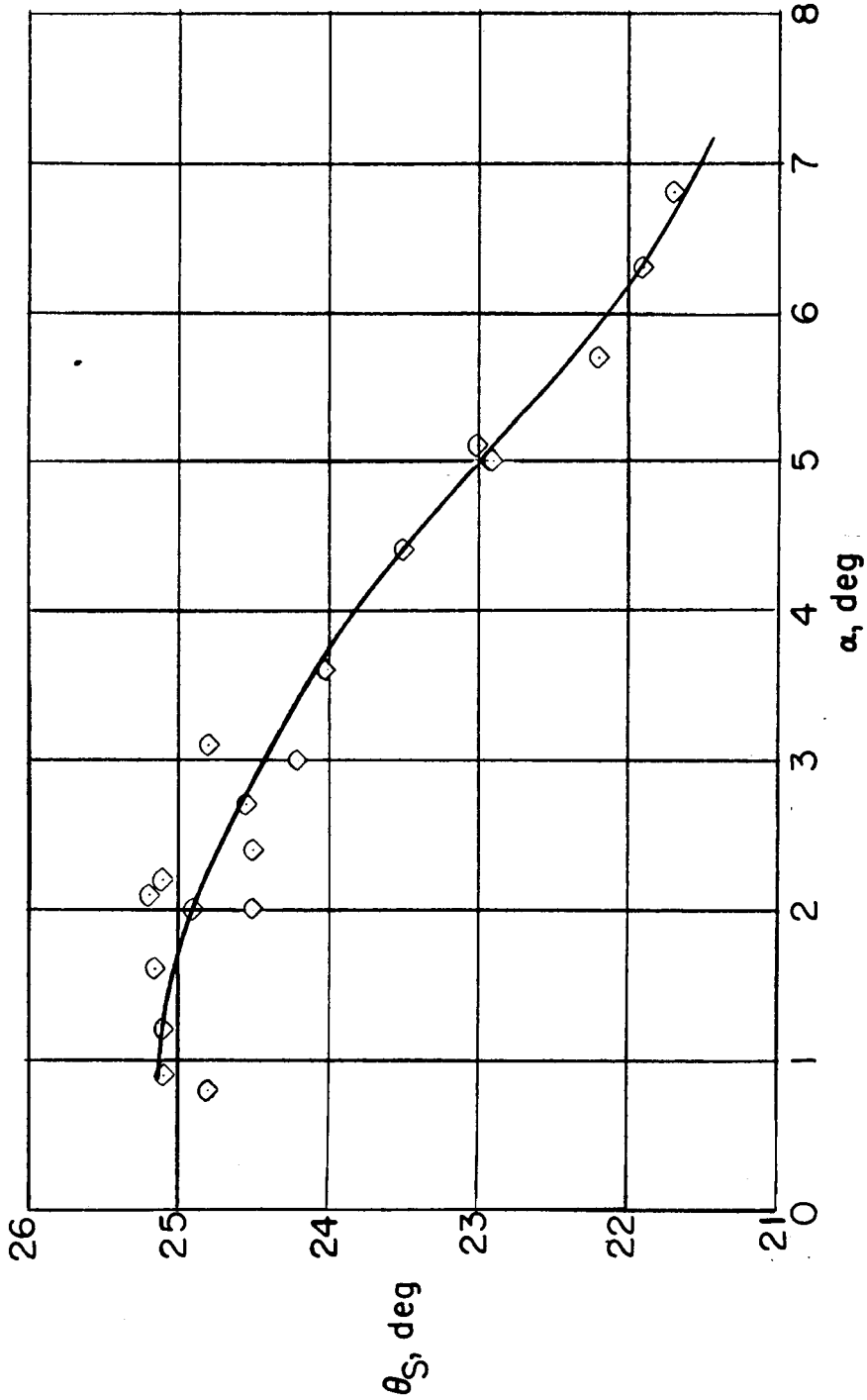


Figure 14.- Area-weighted total-pressure recovery and distortion parameter obtained during a ground run.



(a) Pressure recovery and distortion.
 Figure 15.- Summary of diffuser performance plotted against angle of attack.
 Altitude = 40,000 feet.



(b) Effective conical-compression angle. $M = 1.70$.

Figure 15.- Concluded.

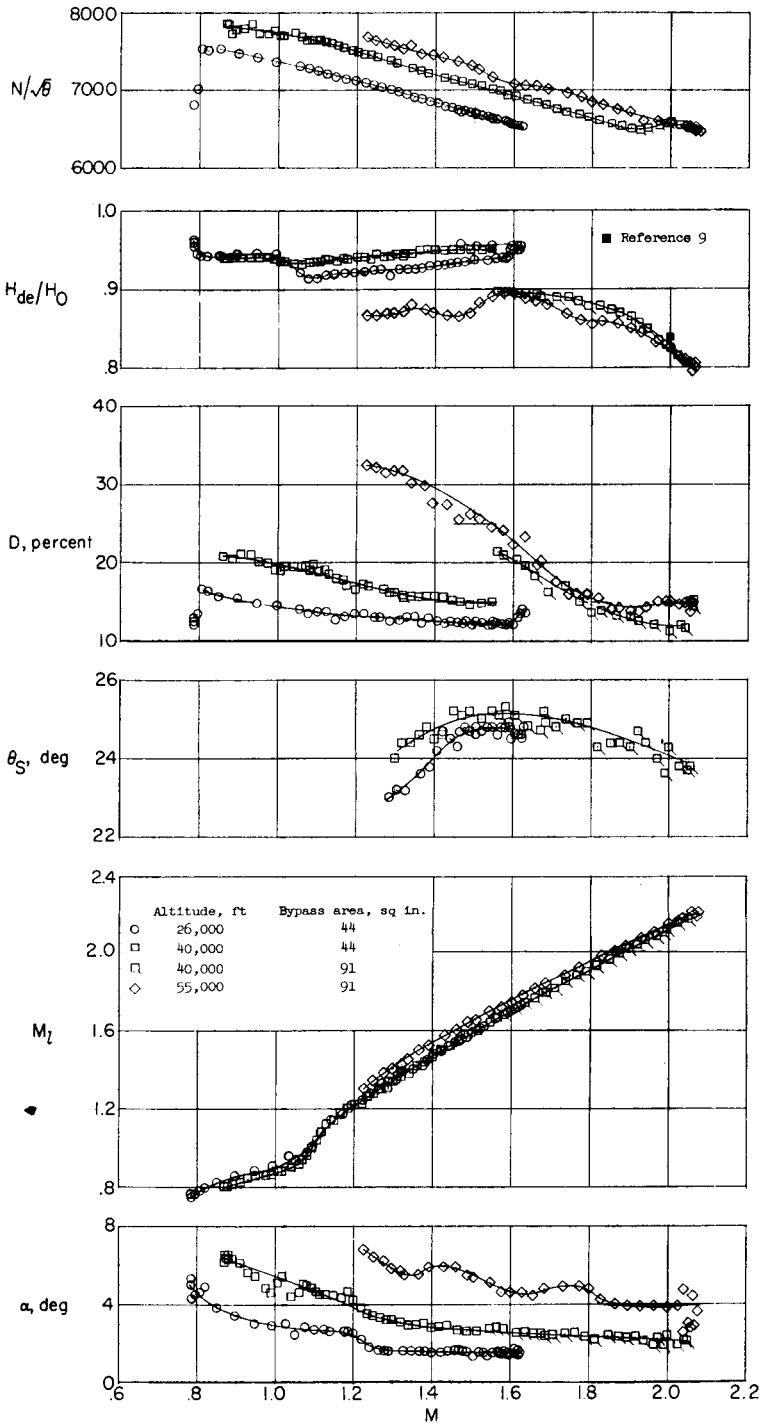
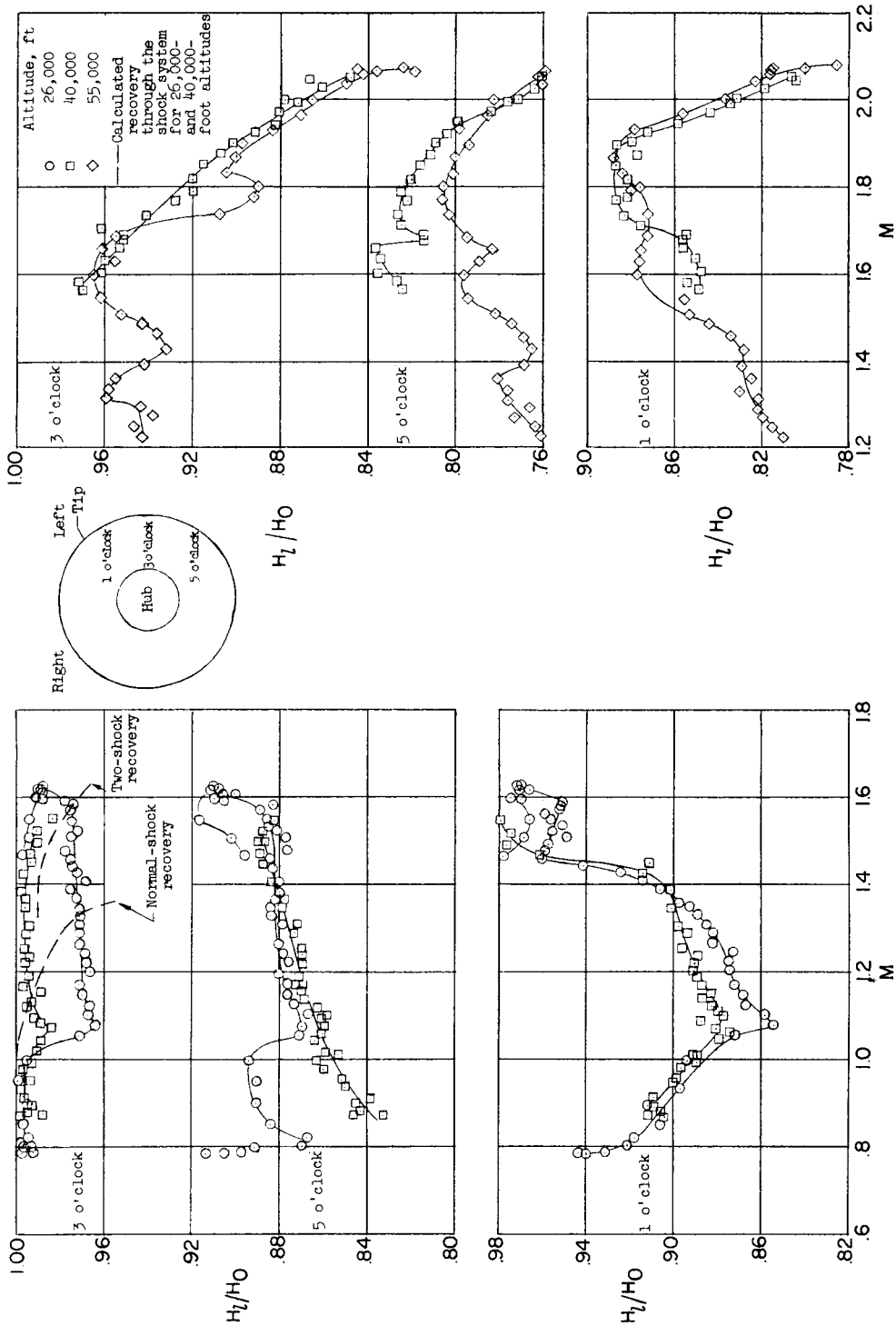


Figure 16.- Summary of several induction-system and airplane parameters plotted against Mach number.



(a) Bypass area = 44 sq in.

(b) Bypass area = 91 sq in.

Figure 17.- Local total-pressure recovery of the left-hand-compressor face.

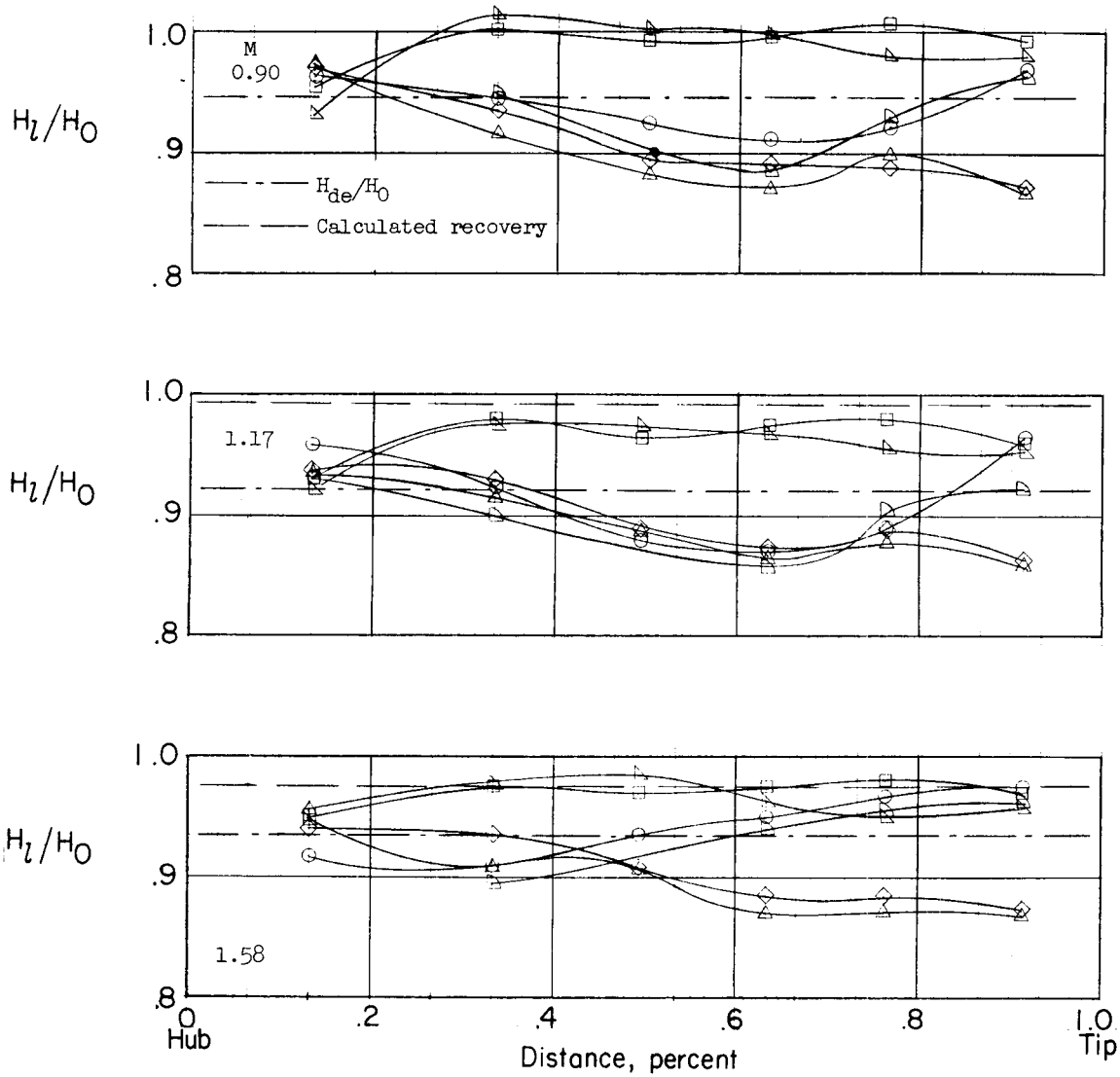
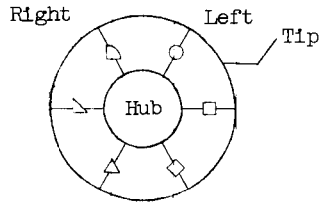
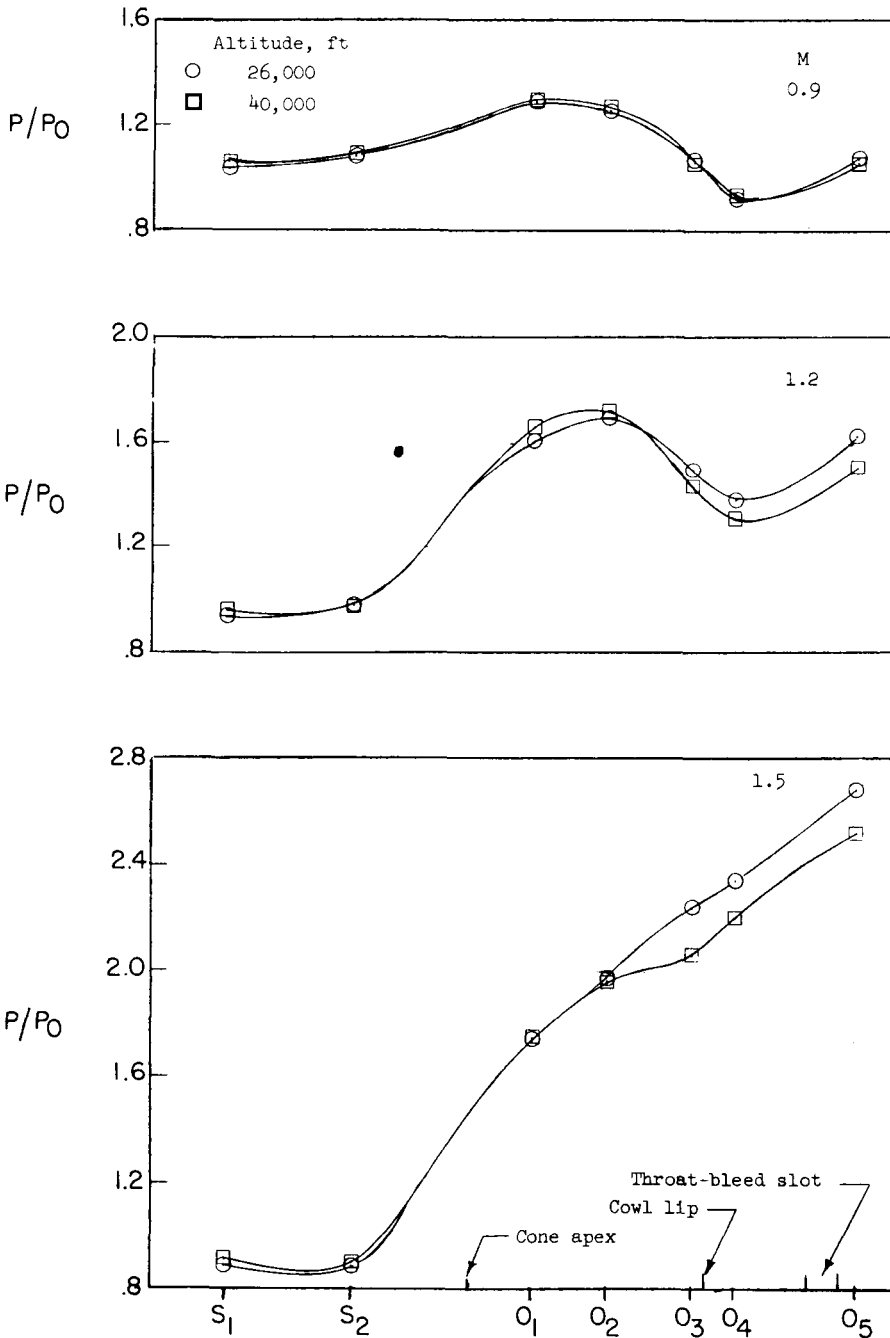
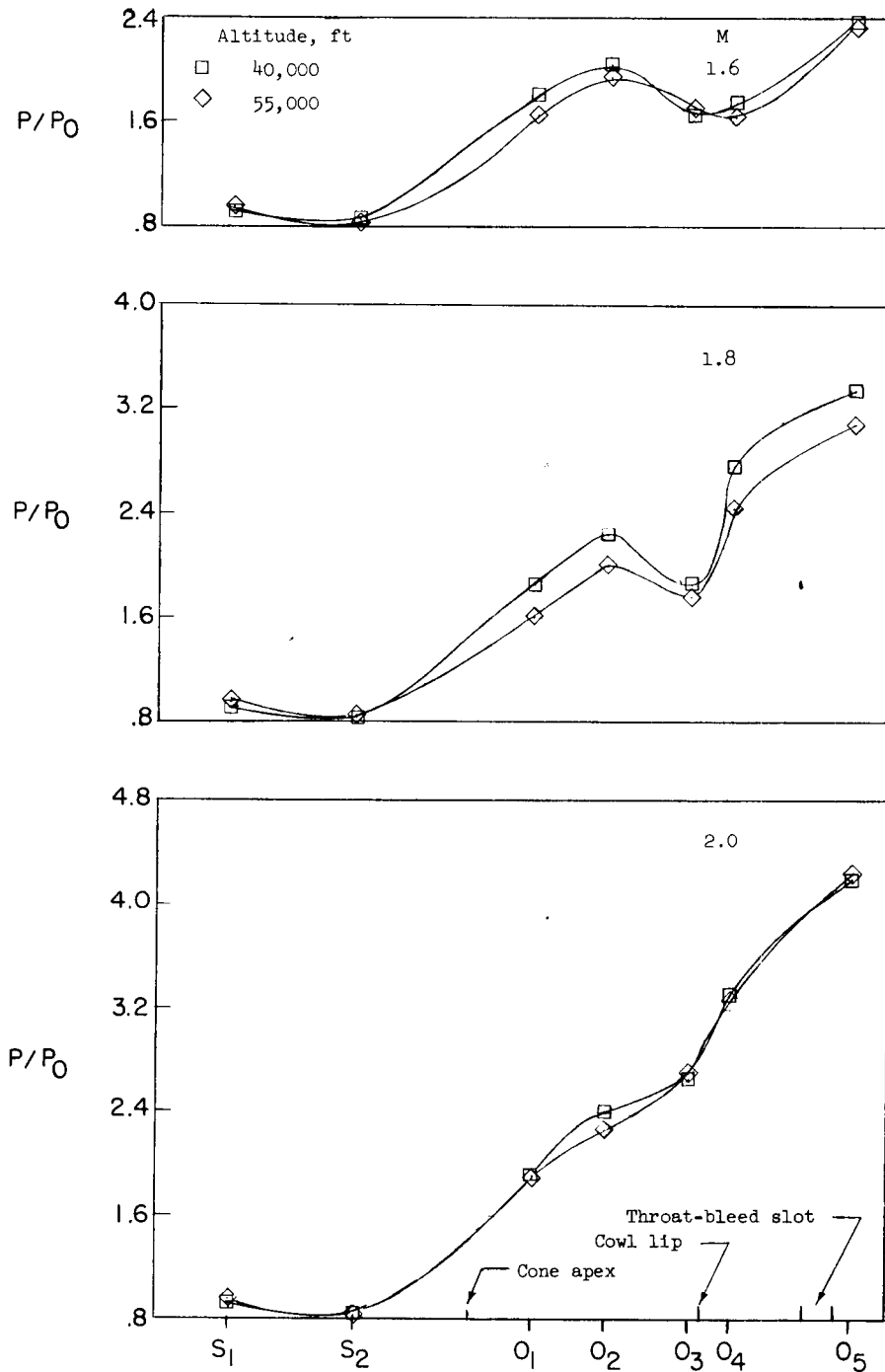


Figure 18.- Local total-pressure recovery.



(a) Bypass area equal to 44 sq in.

Figure 19.- Cone-pressure profile referenced to free-stream static pressure.



(b) Bypass area equal to 91 sq in.

Figure 19.- Concluded.